علماء المستقبل

هذا البرنامج برعاية

مؤسسة عبدالمنعم الراشد الإنسانية
Abdulmonem Alrashed Humanitarian Foundation

kfu.edu.sa

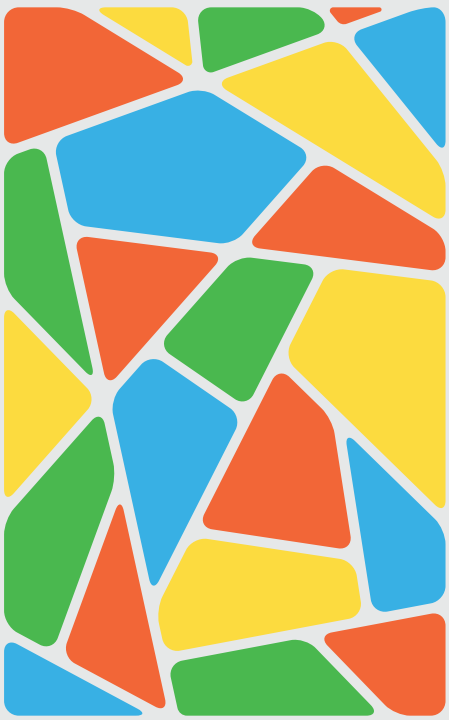

علماء المستقبل

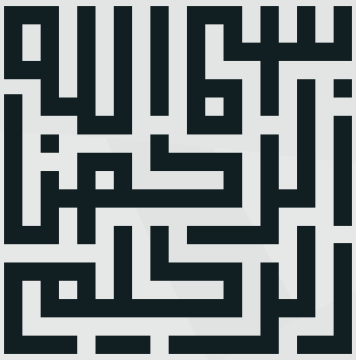

علماء المستقبل
يرحب بكم

التكريم

مقدمة

يهدف البرنامج إلى دمج طلبة الجامعة وطلبة التعليم العام (طلاب/طالبات الثانوي) في مشاريع بحثية تصمم بواسطة أعضاء هيئة التدريس المتميزين ويتم تنفيذها تحت إشراف أعضاء هيئة التدريس بالجامعة والفنيين من كليات مختلفة مثل: العلوم والطب والهندسة والمعامل المركزية؛ وذلك لإكساب طلبة التعليم العام مهارات البحث العلمي وأدواته والتحفيز على الاكتشاف والابتكار بطرق علمية ومنذ وقت مبكر.

برنامج علماء المستقبل يشمل سبعة مسارات هي: مسار الذكاء الاصطناعي في الطب (الجراحة)، مسار طب التخدير، مسار الطاقة المتجددة، مسار الهندسة والتصنيع والبناء، مسار الكيمياء، مسار الفيزياء، مسار التقنية الحيوية.

هذه المسارات تتناسب مع استراتيجية برنامج خادم الحرمين للابتعاث، والتي أطلقها صاحب السمو الملكي الأمير محمد بن سلمان بن عبد العزيز، ولي العهد «برنامج خادم الحرمين الشريفين للابتعاث من خلال ابتعاث الطلاب والطالبات لأفضل المؤسسات التعليمية في العالم في مختلف المجالات والدول حسب التصنيفات العالمية، في إطار رؤية المملكة 2030».

بحسب الإعلان على صفحة الجامعة وفي وسائل التواصل الاجتماعية تقدم للبرنامج عدد يفوق 200 طالب وطالبة، تم فرزهم على ثلاث مراحل واختيار أفضل 63 طالبة/طالبة تم توزيعهم حسب الرغبات في سبعة مسارات بواقع 9 طالب/طالبة في كل مسار

مسارات البرنامج (النسخة الأولى)

شـمل البرنامـج سـبعة مسـارات هـي: مسـار الـذكاء الاصطناعـي فـي الطـب (الجراحـة)، مسـار طـب التخديـر، مسـار الطاقـة المتجـددة، مسـار الهندسـة والتصنيـع والبنـاء، مسـار الكيميـاء، مسـار الفيزيـاء، مسـار التقنيـة الحيويـة

الهدف العام للبرنامج (المسارات السبعة):

- تعليم الطلاب على المعلومات والمفاهيم الاساسية بحسب المسار.

- تنمية مهارات العمل الجماعي عند الطلاب.

- تدريـب الطلبـة علـى السلامـة المهنيـة فـي المعامـل والمختبـرات البيولوجيـة، والكيميائيـة، والفيزيائيـة

- تدريـب الطلبـة علـى أجهـزة القيـاس وكيفيـة اجـراء التحاليـل والتعامـل مـع الاجهـزة البحثيـة

- تنمية المهارات البحثية وكتابة الابحاث العلمية والبوسترات.

- تهيئـة الـطلاب وتحفيزهـم للمشـاركة فـي المسـابقات والمعـارض المحليـة أو الاقليميـة والعالميـة

تسجيل الطلاب واختيارهم

- تقدم للبرنامج اكثر من 200 طالب وطالبة.

- تم عمل العديد من المقابلات للمتقدمين.

- تضمنـت معاييـر الفـرز والمفاضلـة بيـن المتقدميـن : (معـدل آخـر شـهادة و درجـة اختبـار القـدرات و اللغـة الانجليزيـة).

- في المحصلة النهائية تم اختيار 63 طالب وطالبة .

- تـم توزيـع الـطلاب الفائزيـن علـى المسـارات وبحسـب الرغبـات بواقـع 9/ طالب/طالبـة لـكل مسـار

- اجتاز البرنامج ٤٥ طالب وطالبة

مخرجات المسارات

1. بوسترات علمية.
2. أوراق علمية تنشر في اوعية النشر العالمية والمجلات العلمية المحكمة.
3. براءات اختراع.
4. منتجات قابلة للتتجير.
5. المشاركة في المعارض المحلية والاقليمية والدولية.

أولاً: البوسترات العلمية

الذكاء الاصطناعي في الطب (الجراحـــــة)	طب التخدير	الهنـــدســـــة والتصنيع والبناء
2	4	6

الكيمياء	الفيزياء	التقنية الحيوية	الطاقـــة المتجددة
7	6	3	5

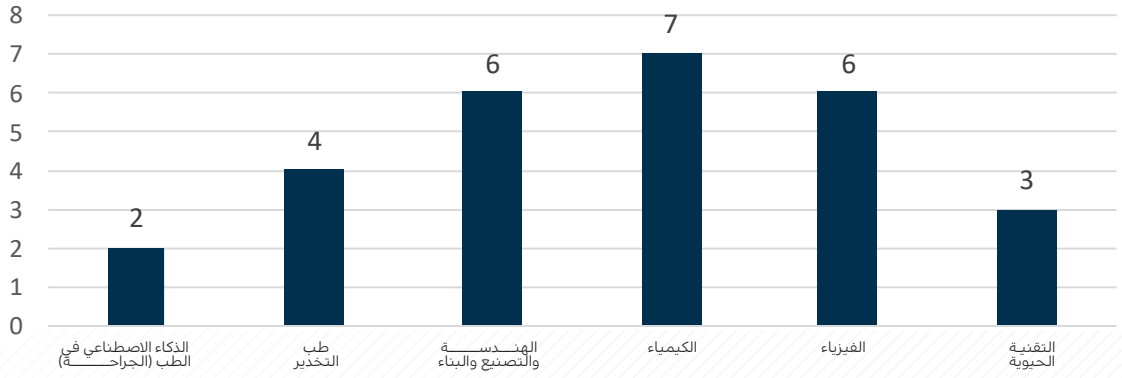

ثانياً: الأوراق العلمية

الذكاء الاصطناعي في الطب (الجراحة)	طب التخدير	الهندسة والتصنيع والبناء
1	2 (عدد الأوراق) / 1 (الأوراق المنشورة)	1

الكيمياء	الفيزياء	التقنية الحيوية	الطاقة المتجددة
2 (عدد الأوراق) / 2 (الأوراق المنشورة)	2	1 (عدد الأوراق) / 1 (الأوراق المنشورة)	2

ثالثاً: براءات الإختراع

الذكاء الاصطناعي في الطب (الجراحة)	طب التخدير	الهندسة والتصنيع والبناء
1	0	1

الكيمياء	الفيزياء	التقنية الحيوية	الطاقة المتجددة
2 (مجال معالجة الماء رقم الطلب 139.461/18 / مجال خلايا الوقود رقم الطلب 33102 29)	0	1	0

رابعاً: المنتجات القابلة للتتجير

الذكاء الاصطناعي في الطب (الجراحة)	طب التخدير	الهندسة والتصنيع والبناء
1	1	2

الكيمياء	الفيزياء	التقنية الحيوية	الطاقة المتجددة
1	0	1	2

برنامج علماء المستقبل
(النسخة الأولى)

معلومات الطلاب/ الطالبات بحسب المسارات:

المسار	السنة الدراسية الحالية	المدرسة	اسم الطالب/الطالبة
مسار الذكاء الاصطناعي في الطب (الجراحة)	ثالث ثانوي	غادرت البرنامج	كيان صلاح ابراهيم المجحد
	ثالث ثانوي	غادر البرنامج	حسن وجيه محمد المسبح
	ثاني ثانوي	مدرسة الكفاح	هدى فراس عبدالعزيز العويفير
	ثالث ثانوي	ثانوية عبد الله بن سلام	احمد موسى احمد الاحمد
	ثالث ثانوي	ثانوية عبد الله بن سلام	علي عبدالواحد عبدالوهاب الخرس
	ثالث ثانوي	مدرسة الأنجال الأهلية	عبدالإله جاسم محمد بوعبيد
	ثاني ثانوي	مدرسة الأنجال الأهلية	فهد عبدالمحسن عبدالعزيز الملحم
	أول ثانوي	ثانوية الإمام جعفر الصادق	عمار محمد عبداللطيف العمير
	اول ثانوي	الثانوية الثامنة بالمبرز	فاطمه عبدالرؤوف عبدالله العامر

مسار طب التخدير	ثاني ثانوي		نوره علي احمد المقرب
	ثالث ثانوي	مدارس الأنجال الأهلية	حسين علي محمد العمران
	أول ثانوي		خوله سعيد محمد بوعينه
	ثالث ثانوي		رضا جميل عيسى الخلف
	ثاني ثانوي	مدارس الأنجال الأهلية	محمد عصام محمد العبدالمحسن
	ثاني ثانوي		رانيه أحمد إبراهيم الحليمي
	ثاني ثانوي		زهراء حسين احمد الموسى
	ثالث ثانوي		يقين حسن ناصر العباس
	اول ثانوي		كادي محمد شميس الحارثي

مسار الكيمياء	ثاني ثانوي		عبدالرحمن عبدالمحسن محمد الموسى
	ثاني ثانوي		فاطمة علي عيسى الخلف
	ثالث ثانوي		فاطمه أيمن عبدالمنعم العيثان
	ثالث ثانوي		مريم بنت عبدالعزيز بن خالد المحيش
	ثاني ثانوي		دانيا أمين عبدالله الغافلي
	ثالث ثانوي		حسين مصطفى منصور الغدير
	ثالث ثانوي		فاطِمة عبدرب الأمير سلمان البوعلي
	ثالث ثانوي		عبدالله مرتضى عبدالوهاب الخرس
			النور يوسف عايش البوصقر

مسار التقنية الحيوية.	أول ثانوي	الانجال الاهلية	اللجين سعيد محمد الوصيبعي
	ثالث ثانوي	النخبة النموذجية	نجلاء عبدالعزيز محمد فهد بن جلوي آل سعود
	ثالث ثانوي	الانجال الاهلية	هيله عادل عبدالوهاب العبيدان
	ثاني ثانوي		فاطمه أيمن عبدالمنعم العيثان
	ثاني ثانوي		خولة يوسف علي السالم
	ثاني ثانوي	التخبة النموذجية	الجوهرة سلطان قاعد المفالحة السبيعي
	ثاني ثانوي	الثانوية الاولى بالمنصورة	أمجاد محمد معتوق الماجد
	ثاني ثانوي		فرح أمين حسين الأمير
	اول ثانوي		آلاء علي جاسر الحربش

مسار الفيزياء.	ثالث ثانوي		عبدالوهاب مصطفى عبدالوهاب القفاص
	ثاني ثانوي		إسراء حسن عبدالله العيسى
			وعد العلي
	ثالث ثانوي		زهراء عماد محمد الغافلي
	ثالث ثانوي		نور عبدالمنعم جواد الدليلي
	ثاني ثانوي		محمد أحمد بن ناصر الحسن
	ثاني ثانوي		رغد عمر عبداللطيف الحمام
	ثاني ثانوي		جُمانة مراد ناصر الناصر
	اول ثانوي		نوف طاهر علي النفيعي

مسار الهندسة والتصنيع والبناء.	ثالث ثانوي		نورة محمد إبراهيم العمر
	ثالث ثانوي		فاطمه اللويم
	ثالث ثانوي	الانجال الأهلية	عبدالرحمن باسم عبدالرحمن الملحم
	ثالث ثانوي	اكاديمية الكفاح	عمر عبدالعزيز عامر العامر
	ثالث ثانوي	الحادي عشر بالهفوف	زينب رفيع عبدالله العليوي
	ثالث ثانوي	الانجال الأهلية	الجوهره صالح ناصر الملحم
	ثاني ثانوي	الانجال الأهلية	منذر جعفر علي الجعفر
	ثالث ثانوي	اكاديمية الكفاح	فيصل محمد ابراهيم الصويغ
	اول ثانوي	الانجال الأهلية	أروى احمد عبدالله الحرز

مسار الطاقة المتجددة.	ثالث ثانوي		غلا حسين بن محمد الفهيد
	ثالث ثانوي		فاطمة علي أحمد الحجي
	ثاني ثانوي		تركي مهناء عبدالله الدلامي
	ثاني ثانوي		عبدالله محمد جمعه السنيني
	ثالث ثانوي		هيثم هادي ناجع التليدي
			رغد المحبوب
	ثالث ثانوي		حسن بن علي بن محمد العمر
	اول ثانوي		حنين محمد أحمد الحسن

المشرفين على مسارات برنامج علماء المستقبل

م	الاسم	الدرجة العلمية	العمادة/الكلية	نوع المشاركة	المسار
1	د. صلاح عبدالغني أحمد الحاشدي	أستاذ مساعد	إدارة المعامل المركزية	مشرف برنامج علمي1	الهندسة والتصنيع والبناء- إدارة سلسلة الإمداد
2	أ.د. خالد محمد أمين رمضان	استاذ دكتور	ادارة المعامل المركزية	مشرف برنامج علمي2	
3	د. فؤاد قاسم الغربي	استاذ مشارك	كلية العلوم	مشرف برنامج علمي1	الفيزياء
4	د. اسامة صابر يحيى محمد	استاذ مشارك	كلية العلوم	مشرف برنامج علمي2	
5	د. اشرف يسن زكي خليفة	استاذ مشارك	كلية العلوم	مشرف برنامج علمي1	التقنية الحيوية
6	د. خير الاسلام محمد ابراهيم	استاذ مساعد	كلية العلوم	مشرف برنامج علمي2	
7	د. هاني محمد عبداللطيف أحمد	استاذ مشارك	كلية العلوم	مشرف برنامج علمي1	الكيمياء
8	د.محمد جوده عبدالحليم محمود	استاذ مشارك	كلية العلوم	مشرف برنامج علمي2	
9	د. محمد عبدالعزيز أحمد العقيل	أستاذ مساعد	كلية الهندسة	مشرف برنامج علمي	الطاقة المتجددة
10	د. اسامه محمد زكريا محمود	أستاذ دكتور	كلية الطب	مشرف برنامج علمي1	الذكاء الاصطناعي في الطب - الجراحه
11	د. محمد ياسر ابراهيم داود	أستاذ مساعد	كلية الطب	مشرف برنامج علمي2	
12	د. خالد أحمد محمد يس	استاذ دكتور	كلية الطب	مشرف برنامج علمي	طب التخدير

المسار الثاني

التقنية الحيوية

مخرجات المسارات

1. بوسترات علمية.
2. أوراق علمية تنشر في اوعية النشر العالمية والمجلات العلمية المحكمة.
3. براءات اختراع.
4. منتجات قابلة للتتجير.
5. المشاركة في المعارض والمؤتمرات المحلية والأقليمية والدولية.

أولاً: البوسترات العلمية

م	المسار	عدد البوسترات
1	الذكاء الاصطناعي في الطب (الجراحة)	**2**
2	طب التخدير	**4**
3	الهندسة والتصنيع والبناء	**6**
4	الكيمياء	**7**
5	الفيزياء	**6**
6	التقنية الحيوية	**3**
7	الطاقة المتجددة	**5**
	اجمالي البوسترات	**33**

Experimental evaluation of antioxidant and anticancer activi for Thyme essential oils extracted by different techniques

Aljawharah Saleh Nasser Almulhim
Prof. Dr. Khaled Ramadan and Dr. Sallah A. A. Al-Hashedi
Engineering and Manufacturing Track

Abstract

Results

Introduction

Materials and Methods

Discussions

Conclusion

References

Separation , elucidation, antioxidant and anticancer activity evaluation for clove essential oils

Faisal Mohammed Al Sowayigh
Prof. Dr. Khaled Ramadan and Dr. Sallah A. A. Al-Hashedi
Paper
Engineering and Manufacturing Track

Abstract

Results

Introduction

Discussions

Conclusion

References

A CODE FOR THE MASS ATTENUATION COEFFICIENTS OF THE GAMMA RAYS IN HUMAN TIUSSUES

Raghad-Alhumam
Supervision : Foued -Gharbi
College of Science/ Department of Physics

Abstract

Gamma-ray mass attenuation coefficient for Lung and brain tissues, have been calculated using the Monte Carlo simulation Geant4 for energy less than 2 MeV. The obtained μ/ρ values were validated by comparison with experimental and theoretical XCOM results, as well as compared to values found by other authors using Geant4 and MCNP codes. Our developed code can be used as efficient alternative to experimentation when chemical composition of the human tissue is known.

The mass attenuation coefficient μ (cm²/g) is a key factor for evaluating the effect of gamma radiation at appropriate energy with the studied material and can be deduced from Beer-Lambert Law according to :

$$\mu = -\frac{1}{\rho x}\ln\left(\frac{I}{I_0}\right) = \frac{N}{N_0}$$

XCOM
Comparison between mass attenuation coefficients for the human tissues using XCOM software online and Geant4 code at various photon energies.

Introduction

Discussion

Obtained results

Materials and methods

Conclusion

References

Experimental evaluation of antioxidant and anticancer activity for Basil essential oils

Arwa Ahmad Abdullah Alherz
Prof. Dr. Khaled Ramadan and Dr. Sallah A. A. Al-Hashedi
Engineering and Manufacturing Track

Abstract

Results

Introduction

Discussions

Conclusion

References

Antibacterial activity of basil essential oil (*Ocimum basilicum*) against foodborne pathogens

Omar Abdulaziz Amer Al-Amer

Dr. Sallah A. A. Al-Hashedi and Prof. Dr. Khaled Ramadan

Paper

Engineering and Manufacturing Track

Abstract

Background and Aim: Sweet basil (*Ocimum basilicum* L.) has been used as a traditional medicinal plant, whereas essential oils of basil (EOBs) used as antimicrobial activity against a wide range of Gram-negative and Gram-positive bacteria, yeast, and mold. This study aimed to determine the antibacterial activity of basil (*Ocimum basilicum* L.) essential oils against foodborne diseases bacteria or pathogens bacteria and some of lactic acid bacteria such as Lactococcus lactis subsp. lactis.

Results: Essential oils of sweet basil (*Ocimum basilicum* L.) has biological activity, exhibited inhibitory effects toward tested pathogens microorganisms and foodborne diseases such as *Listeria monocytogenes*, *Staphylococcus aureus*, *Pseudomonas aeruginosa*, *Salmonella enterica* and was inhibitory effects toward all lactic acid bacteria or probiotic bacteria such as *Lactococcus lactis* subsp. *lactis*, *Leb. delbrueckii* subsp. *bulgaricus* and *Streptococcus thermophilus*.

Conclusion: Antimicrobial activity test (using well assay in vitro) suggests that EBOs possess good antibacterial activity against a wide range of foodborne pathogens, and less microbial activities for probiotic bacteria or lactic acid bacteria LAB.

Keywords: basil (*Ocimum basilicum*), essential oils, *Listeria monocytogenes*, *Pseudomonas aeruginosa*, well assay

Introduction

Ocimum basilicum L. (sweet basil) belongs to the family Lamiaceae, which includes about 200 species, commonly known as sweet basil, has been used as a traditional medicinal plant for the treatment of headaches, coughs, diarrhea, constipation, warts, worms, and kidney malfunctions (Joshi, 2014; Simon et al., 1999). Holy basil (*O. sanctum*), Sweet or Thai basil (*O. basilicum*), Lemon basil (*O. citriodorum*), and Tree basil (*O. gratissimum*) are frequently cultivated in several countries of South and South-East Asia including Thailand as culinary herbs (Juntachote et al., 2006; Mahajan et al., 2012). Basil essential oils (EOs) have been used extensively for many years in food products, perfumery, and dental and oral products. EBOs are antimicrobial activity against a wide range of Gram-negative and Gram-positive bacteria, yeast, and mold (Suppakul et al., 2003).

Basil essential oils (EOs) are natural volatile compounds and contain a wide range of chemical constituents produced by plant secondary metabolism (Ibi et al., 2019) and used for applications in various industries such as pharmaceutical (Srivastava et al., 2017), cosmetic, perfumery, dental, and oral products (Suppakul et al., 2003) and the aromatherapy and food industries (Pezzoa et al., 2013). Basil has been applied in traditional medicine with positive effects against fever and cough, flu, asthma, and bronchitis (Shahrajabian et al., 2020). Basil used in the Balkan diet is described as having radio-protective, anti-inflammatory, anti-stress, anti-diabetic, and anti-pyrexic properties (Ibi et al., 2019).

Materials and Methods

1. Bacterial strains

Bacterial strains (ATCC and DSM strain) used as indicators for basil essential oil evaluation for antimicrobial activities are shown in Table (1). Lactic acid bacteria (LAB) reference strains, were propagated in MRS broth (Oxoid, UK) at 37°C ±1 °F for up to 48 h and pathogenic bacteria (indicators) were activated in Brain Heart Infusion (BHI) broth (Oxoid, UK) at 37°C ±1 °F for 24h ±2. Working culture (LAB and other indicators) were maintained at 5°C in MRS+1.5% agar (loop agar for LAB) or slants of BHI +1.5% agar for pathogens strains.

2. Evaluation of different concentrations of basil essential oil for antibacterial activity in vitro

Antimicrobial activity for BEO were screened using the agar well diffusion test of Nzeako et al. (2006). Sterilized 100 ml nutrient Agar (Oxoid, UK) were tempered to 48°C (in water bath) prior to seeding with 100µl (10^8 CFU/ml) of diluted culture from the indicators listed in Table (2). Inoculated media were poured into Petri plates (in replicate) then left to harden under room temperatures. Wells (6 mm in diameter) were made in the agar with a sterile Cork borer and each well was filled with 100µl of BEO. Inhibition zones (including well diameter) around wells were measured in mm after incubation at 37° C. Clear zones greater than 8 mm were considered as active BEO against the indicator. Zones of inhibition were measured and the average zone size of each dilution was taken.

Results

Table (1). Indicator bacteria used in the study

Bacteria	Code number
Leuconostoc mesenteroides subsp. *dextranicum*	DSM 20484
Lactobacillus delbrueckii subsp. *lactis* (*Leb. lactis*)	ATCC 19435
Lactobacillus delbrueckii subsp. *bulgaricus* (*Leb. bulgaricus*)	ATCC 11842
Lactobacillus acidophilus	ATCC 4356
Lactobacillus casei	ATCC 393
Lactobacillus plantarum	ATCC 8014
Streptococcus thermophilus	DSM 20617
Pediococcus acidilactici	ATCC 8042
Lactococcus lactis subsp. *lactis*	ATCC 19435
Lactococcus lactis subsp. *cremoris*	ATCC 19257
Bacillus cereus	ATCC 14579
Staphylococcus aureus	ATCC 6538
Escherichia coli	ATCC 25922
Salmonella enterica	ATCC 13076
Pseudomonas aeruginosa	ATCC 27853
Listeria monocytogenes	ATCC 19115

Table (2). Sensitivities of Reference bacteria to basil essential oil (BEO) using the well-assay inhibition zones (mm)

Bacteria	Pathogenic bacteria (Laboratory diseases)				Lactic acid bacteria			
	Gram-negative bacteria		Gram-positive bacteria					
	ARCTC	PAO1	RN 4220	DSM5	NA65	L.del.	L.plan.	BLIS
BEO µl								
400 µl/l	+++	+++	+	+	+ + +	+	+	+
200 µl/l	+	+	-	-	+ +	-	-	-
100 µl/l	-	-	-	-	+	-	-	-
50 µl/l	-	-	-	-	-	-	-	-
25 µl/l	-	-	-	-	-	-	-	-
12.5 µl/l	-	-	-	-	-	-	-	-
6.25 µl/l	-	-	-	-	-	-	-	-
3.12 µl/l	-	-	-	-	-	-	-	-
1.56 µl/l	-	-	-	-	-	-	-	-
0.78 µl/l	-	-	-	-	-	-	-	-
0.39 µl/l	-	-	-	-	-	-	-	-
0.19 µl/l	-	-	-	-	-	-	-	-
0.09 µl/l	-	-	-	-	-	-	-	-

Inhibition zones (mm) for antibiotic disc against reference bacteria.

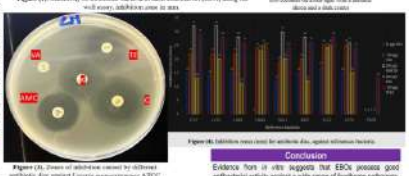

Figure (A). Zones of inhibition (mm) by different antibiotic disc against *Listeria monocytogenes* ATCC 7644, using disc diffusion assay.

Figure (B). Inhibition zones (mm) for antibiotic disc against reference bacteria.

Discussions

Basil essential oils contains a wide range of chemical compounds, whose content may vary depending on chemotypes, environmental conditions, agronomic techniques and particularly the origin of the plant (Ibi et al., 2019).

Resistance to antibiotics is increasing globally, and at a very alarming rate. In general, bacteria have the genetic capacity to both gain and transmit resistance to drugs used as therapeutics. Extending the useful life of current antimicrobials might be possible if they were used in combination with natural products. These combinations could represent therapeutic alternatives for the treatment of infections (Maurmez & Berberis 2020; Stuart & Bonne 2004).

Basil essential oil exhibited antimicrobial activity surpassing the activity of relevant commercial antibiotics regardless of growing conditions in the case of *B. cereus*, *K. pneumoniae* and *C. albicans* while superior antimicrobial activity was exhibited in the case of essential oils from plants grown under blue nets in the case of *S. aureus*, *E. coli* and *P. vulgaris* (Ibi et al., 2019).

Conclusion

Evidence from *in vitro* suggests that EBOs possess good antibacterial activity against a wide range of foodborne pathogens. The essential oils of basil (*O. basilicum* may be applied as a natural antimicrobial agent. Among all tested strains, the most sensitive to BEO were: *Listeria monocytogenes*, *Staphylococcus aureus*, *Pseudomonas aeruginosa*, *Salmonella enterica* and the resistant strains were: *Leb. delbrueckii* subsp. *bulgaricus*, *Lactococcus lactis* subsp. *lactis*, *Streptococcus thermophilus*, *Staphylococcus saprophyticus*. The obtained results are useful in the search of more selective and naturally produced antimicrobial compounds.

References

M. Ali, Basil (*Ocimum basilicum* L.): A Review, Ph. [illegible] Chemical constituents of the essential oil of *Ocimum basilicum* L. cultivated in Hong Kong, Int. [illegible] Nutritive Value of Basil (*Ocimum basilicum* L.), J. Food Nutr. Res. [illegible] Chemical composition and antimicrobial activity of the essential oil of *Ocimum basilicum* L. (sweet basil) from Western Ghats of North India, J. Agric. Food Chem. [illegible] Antibacterial activity of *Ocimum basilicum* L. essential oil, Flavour Fragrance J. [illegible] Antimicrobial activity of basil (*Ocimum basilicum* L.) essential oils against foodborne diseases bacteria or pathogens bacteria and some of lactic acid bacteria such as Lactococcus lactis subsp. lactis, Biocatal. Agric. Biotechnol. [illegible] Antibacterial activity of basil essential oil (*Ocimum basilicum* L.) against multi-drug resistant clinical pathogens, Phytomedicine [illegible] Antimicrobial activity of basil (*Ocimum basilicum* L.) essential oil against foodborne pathogens, Int. J. Food Microbiol. [illegible] Antimicrobial activity of basil (*Ocimum basilicum* L.) essential oil against foodborne pathogens, Int. J. Food Microbiol. [illegible] Antimicrobial activity of basil (*Ocimum basilicum* L.) essential oil against foodborne pathogens, Int. J. Food Microbiol. [illegible] Antimicrobial activity of basil (*Ocimum basilicum* L.) essential oil against foodborne pathogens, Int. J. Food Microbiol.

Future Scholars Program 2023

برنامج علماء المستقبل 2023

Artificial intelligence aided in medicine

Reliably of Artificial Intelligence (AI) programs in proper wound measurement during disasters

Kadi Alharthi, Fatimah Alamer, Huda Alowifeer

Professor. Ossama Zakaria

Abstract

Artificial intelligence has gained more popularity in many life fields within the last decades. It has proven to be very successful in medicine and surgery. It proved to be highly sensitive in the diagnosis and treatments of many situations. This project aims to indulge the AI program with a very primitive form of Arduino drived software robot as an experimental trial to deal with wounds and burns during emerging disasters situations.

Introduction

Disasters constitute a very challenging problem for mankind. This may lead to many health problems that need to be immediately dealt with to overcome morbidities and mortalities. Nevertheless, human beings might sometimes be in great danger if they will deal with such problems. Robots have been proven to replace humans during similar situations such as the covid 19 pandemic. Artificial intelligence has added much information to deal with many medical situations, notably, wounds and burns. The current preliminary project was designed to test the efficacy of integrating a primitive robot that is AI aided medical and surgical catastrophes.

Materials and Methods

We adopted a primitive form of the robot (Arduino). It is mobilized by a remote control. It is having a mobile camera. This mobile camera would take photos and send them to the AI program to be compared with the previously fed images. Obtain the results would be notified and accordingly dealt with the program. A Special designed AI program was set to diagnose different categories of wounds and burns-related disasters. Five main categories would be studied included cut wounds, superficial and deep ulcers, burns, and contused wounds. AI data banks of these different categories would be set. Photographically taken data would be sent via Wi-Fi to the computer (aided mobile software and/or laptops, or desktops). Data would be interpreted as regards the reliability or validity of the technique. Statistical analysis would be used to measure the success of the AI program.

Results

Wound type	Reliability
Burn	99%
Superficial wounds	98%
Deep wounds	96%
Contused wounds	98%
Cut wounds	97%

The taken photos were more than 550 photos

Discussions

Needs are is the drive for innovations. Through time, war has aided in the discovery of many surgical technical adventures. Therefore, wars and disasters which are two faces of the same coin have led to the acceleration of many advances in wound care and trauma management with enormous investments. Recently, artificial intelligence plays a crucial role as a predictor and analytic successful tool in surgical triages on battlefields. AI is not only used for wound assessment but also may be used as a successful tool for burn victims by governing those who require immediate surgical intervention. This has led to overcoming the shortage of burn specialized surgeons during wartime. Such machine-learning techniques were successfully tried during the latest Russian-Ukrainian war. The technique mainly relies on using multispectral images that are AI integrated as algorithms. This may help to distinguish between damage and health tissues. This technique is fast, visible, and reliable. It takes not more than 0.2 seconds. Moreover, it is superior to humans with the sense of exploring the whole layers of the burned skin in construct to the limitation of the naked-eye's ability. The AI technology in the management of wounds and burns is still considered under trial. Therefore, our current program is considered a recent and highly innovative experimental tool to deal with such disasters.

Conclusion

The proposed artificial intelligence program seems to be highly effective and influential in the management of emergency disasters- related surgical situations. The number of used data is limited. Hence, further studies with larger cohorts may be needed for more precise information.

References

Future Scholars Program 2023

برنامج علماء المستقبل 2023

Assessment of Natural Radioactivity in soil samples from King Faisal University and their radiological characterisation.

Noor Al-Dalili

Supervision : Dr. Foued Gharbi

College of Science/Department of Physics

Abstract

The activity concentration and the gamma absorbed dose rates of the terrestrial naturally occurring radionuclides (^{226}Ra, ^{232}Th, and ^{40}K) were determined in soil samples collected from 12 different locations of King Faisal University in Al-Ahsa. Radioactivity concentration (in Bq/kg) was measured using a NaI gamma-ray spectrometer for all the collected samples. *Results:* The concentrations of ^{226}Ra, ^{232}Th and ^{40}K were found ranging from 13.6 (sample 2) to 28.6 (sample 4) Bq/kg and from 11.2(sample 9) to 24.5 (sample 7) Bq/kg and 245.6 (sample 12) to 561.6 (sample 4) Bq/kg with overall mean values of 23.11 Bq/kg, 17.48 Bq/kg, and 373.14 Bq/kg , respectively. The mean radium equivalent (Ra_{eq}) and outdoor radiation hazard index (H_{ex}) for the area under study were found equal to 69.51 Bq/kg and 0.20 respectively. *Conclusion:* The obtained radiological indices values were less than their maximum recommended permitted values. This confirms that the soil of King Faisal University is safe from the radioprotection point of view.

Introduction

Human are permanently exposed to ionizing radiations emitted from natural and man-made sources. Natural radiation originates from the interaction of cosmic ray particles with the atmospheric elements and naturally occurring radioactive elements found in the earth's crust. Soil is one of the sources which could contaminate the environment when containing high levels of natural radioactivity. The determination of the radiological characteristics of the soil is based on the measurement of the activity concentration of the three radioisotopes ^{232}Th, ^{226}Ra and ^{40}K in soil. Their determination allows to assess the radiation exposure to the well defined radiological indices. These indices are the: Radium equivalent activity, External hazard index, Internal hazard index, Indoor air absorbed dose rate and the External hazard index. In this work Nal gamma spectrometry was used to measure the concentration of these radioisotopes in a collection of 12 samples taken from different regions within King Faisal University in Al-Ahsa region in Saudi Arabia. The measured activities were used to determine the radiological characterization of the samples, which allowed to decide about their radiological safety.

Materials and Methods

12 soil samples were collected from different locations at King Faisal University. The samples were oven dried at a temperature of 105°C for 12 h, sieved through a 200 mesh and conditioned in polyethylene containers of 100 cm^3 volume. Each sample was left 4 weeks before acquisition to allow for the establishment of the secular equilibrium between ^{226}Ra and ^{232}Th and their progenitors. Measurement of the activity was performed with a 3x3 inch NaI scintillation detector employing a lead shielding to reduce the penetration of the measurement process by the Background radiation. In order to reduce more the effect of the background radiation on many geometry acquisition was performed for a duration of 300000 s and the obtained spectrum was subtracted from the spectra relative to the samples. SciintiVision Orsac Software was used to calibrate the detector and to measure the count rate relative to each emission energy of interest in the obtained spectra.

Results

Table 1. Obtained activity concentrations and calculated radiological indices:

Samples	^{226}Ra (Bq/kg)	Uncertainty	^{232}Th (Bq/kg)	Uncertainty	^{40}K (Bq/kg)	Uncertainty	Ra_{eq}	H_{ex}	I_γ
S1	20.1	2.1	15.1	1.6	344.1	36.1	0.0753	0.0203	0.0545
S2	13.6	1.4	11.2	1.2	245.6	25.8	0.0511	0.0138	0.0369
S3	27.1	2.8	21.1	2.2	370.1	38.8	0.0967	0.0261	0.0700
S4	28.6	3.0	22.3	2.3	561.6	58.9	0.1178	0.0318	0.0853
S5	19.1	2.0	14.9	1.6	343.1	36.0	0.0744	0.0201	0.0539
S6	19.6	2.1	15.3	1.6	352.1	37.0	0.0764	0.0206	0.0554
S7	24.1	2.5	18.8	2.0	433.1	45.5	0.0940	0.0254	0.0681
S8	20.1	2.1	15.7	1.6	361.1	37.9	0.0783	0.0212	0.0568
S9	13.6	1.4	11.2	1.2	245.6	25.8	0.0511	0.0138	0.0369
S10	20.1	2.1	15.7	1.6	361.1	37.9	0.0783	0.0212	0.0568
S11	20.1	2.1	15.7	1.6	361.1	37.9	0.0783	0.0212	0.0568
S12	28.6	3.0	22.3	2.3	561.6	58.9	0.1178	0.0318	0.0853
Average	20.1	2.1	15.7	1.6	373.1	39.2	0.0783	0.0212	0.0568

Fig 1. Gamma-ray NaI(Tl) scintillation detector and samples soils

Fig 2. Area of study

Discussions

Activity concentrations of the natural radionuclides were measured for the collected soil samples. The activity concentrations of ^{226}Ra, ^{232}Th, and ^{40}K radionuclides for the soil samples are calculated and presented in Table 1. Fig 4. shows a comparison of the obtained mean activity concentrations values of ^{226}Ra, ^{232}Th, and ^{40}K (Bq/kg) with the mean values from soils of different regions of Saudi Arabia [1,8]. Activity concentration is determined through using equation :

$$A(Bq/kg) = \frac{N_1}{T_1}\frac{N_2}{T_2}\frac{1}{\varepsilon P_\gamma m}$$

Where :

N_1 the count number during the acquisition time; T_1 in second of the sample, N_2 the count number during the acquisition time T_2 in second of the Background, ε the full energy peak efficiency of the detector, P the emission probability and m the mass in kg of the sample.

The radiological index Ra_{eq} is determined according to [4]:

$$Ra_{eq}\left(\frac{Bq}{kg}\right) = A_{Ra} + 1.43A_{Th} + 0.077A_K$$

All the obtained Ra_{eq} values (see table 1) are significantly less than the recommended safe limit value 370 Bq/kg. The mean value of Ra_{eq} obtained for the soil samples is 69.93 Bq/kg. It is very low compared to the safe limit recommended value.

The external hazard index for samples under investigation is given by the following equation [2]:

$$H_{ex} = \frac{A_{Ra}}{370} + \frac{A_{Th}}{259} + \frac{A_K}{4810}$$

In addition, the external irradiation radon and its short-lived products are also hazardous to the respiratory organs. The values of outdoor radiation hazard index (H_{ex}) vary from 0.17 to 0.25 with a mean value of 0.2. All the obtained values are less than the critical value of unity. Therefore, based on these results of radium equivalent activity and external hazard indices, one can conclude that there is no health hazard from the soil of Al-Ahsa region. External and internal hazard indices were also calculated for soils. The health hazard for the population in the environment results mostly from the alpha-radioactive nuclides being present in air. To estimate the population internal exposure associated with the natural radio nuclides in soil, the internal hazard index (H_{in}) was calculated according to equation [3]:

$$H_{in} = \frac{A_{Ra}}{185} + \frac{A_{Th}}{259} + \frac{A_K}{4810}$$

The criterion of this model considers that the maximum value of H_{in} is equal to unity. The values of indoor radiation hazard index (H_{in}) vary from 0.22 to 0.33 with a mean value of 0.26, which is less than the critical value of being less than unity (See table 1).

The gamma index I_γ was calculated according to equation [4] :

$$I_\gamma = \frac{A_{Ra}}{150} + \frac{A_{Th}}{109} + \frac{A_K}{1500} \leq 1$$

Its maximum recommended limit is 2 to fulfil the requirement of radiological safety. All the obtained values of this index for all the soil samples studied in this work were significantly less than 2 (Column 8 of table 1). Notably, I_γ was found to be between 0.03 and 0.07

Conclusion

It is important to determine background radiation levels in order to evaluate the health hazards. Gamma spectrometry had been used in this work to measure the radioactivity concentrations of 12 soil samples collected from different locations of King Faisal University in Al-Ahsa. It was found that the mean activity concentrations of ^{226}Ra, ^{232}Th, and ^{40}K are equal to 23, 17 and 373 Bq/kg, respectively. The study showed that the measured values are less than worldwide values. External hazard indices were found to be less than the maximum acceptable limits. Therefore, the study area is within the zone of normal radiation level, which means that the soil radioactivity of King Faisal University is safe from the radioprotection point of view. However, the data provided in this study, offer a background level for the area studied and may also serve as a guideline for future measurement and assessment of possible radiological risks to human health in this region.

References

[1] K. S. Al Mugren, Assessment of Natural Radioactivity Levels and Radiation Dose Rate in Some Soil Samples from Hotwheat Area, AL-HASA/AR Saudi Arabia, Natural Science, 2010, 7, 120-127.

[2] Krieger, R. (1981). Radioactivity of Construction Materials. Betonwerk und Fertigteil-Technik/Concrete Precasting Plant and Technology, 47, 468-473.

[3] Veiterich, L., and Nirdi, M.R. (1987) Natural Radioactivity of Some Brazilian Building Materials. Radiation Protection Dosimetry, 74, 227-229.

[4] Nuclear Energy Agency (OCDE) Exposure to radiation from the natural radioactivity in building materials report. OECD

Future Scholars Program 2023

برنامج علماء المستقبل 2023

Correlation and agreement of hemoglobin concentration measured with non-invasive spectrophotometric method to hemoglobin concentration measured with cell analyzer in sickle cell disease patients. A diagnostic test accuracy

دراسة تشخيصية و دقيقة للقياس غير الغازي لتركيز الهيموجلوبين بالدم و علاقته و دقته مع القياس المعملي في مرضى ذوي الدم المنجلي

رانيه أحمد الحنيص الكبيسيه التفاح الأهليه

محمد عصام العيد المحسن مدارس الأجيال الأهليه

ممرار طب التشخير

خالد أحمد بن وشحة آل قبيل

أستاذ التشخيص الطبي وعلمية أمراض الدم

Hereditary Blood Disease Center Research Team:

Fatimah Alfahal, Nawal Elbayli, Abdulaziz Basheikh

Statistics KPU: Sayed Ali

Introduction

- Non-invasive monitoring can help in the management of patients suffering from Sickle cell disease (SCD) and reduce blood sampling.
- Aim is to monitor noninvasive spectrophotometric haemoglobin (SpHb, g/dl) concentration among SCD patients during their routine clinic visit and study their correlation and agreement with laboratory haemoglobin (Hb, g/dl).

Materials and Methods

- Approved by Al-Ahsa health Cluster (IRB KTHI) No H-05-HS-065) IRB Log No: 06-UP-2023.
- Patients with SCD visiting the Hereditary blood disease center in Al-Ahsa for follow up were included.
- SpHb, Pleth variability Index (PVI, %) and Perfusion Index (PI) measured via finger probe sensors (Masimo Radical 7, Irvine, CA, USA).
- PPI values range from 0.02% for very weak pulse to 20% for extremely strong pulse.
- PI = AC/DC x 100% and by using PI, PVI is calculated
- PVI = PImax - PImin/ PImax X 100%.
- Laboratory Hb measured by Abbott CELL-DYN Ruby hematology analyzer (Abbott, Abbott Park, Illinois, USA).
- Study time: During routine follow-up visit to the clinics. P < 0.05 indicates statistical significance.

Masimo Radical 7 bedside monitor

Abbott CELL-DYN Ruby hematology analyzer (Abbott, Abbott Park, Illinois, USA)

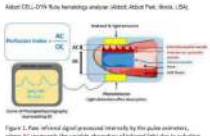

Figure 1. Pulse oximetry signal processed internally by the pulse oximeters, where AC represents the variable absorption of infrared light due to pulsating arterial inflow and DC represents the constant absorption of infrared light due to skin and other tissues.

Results

- 139 patients enrolled (26th Jan 2023 - 1st May 2023), Table 1. Represents demographics, SpHb (g/dL), lab Hb (g/dL), PVI (%) and PI
- A positive correlation existed between Hb (g/dl) and SpHb (g/dl). Kendall's tau correlation (τ) (n=158, τ = 0.68, p< 0.001), Figure 2.
- A good degree of reliability observed between Hb (g/dl) and SpHb (g/dl) (n=151 readings) Intra Class Correlation (ICC) was 0.671 and 95% CI 0.57-0.741, p<0.001, Figure 3.
- High mean PVI was 16.72 ± 7.09 % and low mean (SD) of Perfusion index (PI) was 2.52±1.7. The PI, a quantitative measure of perfusion significantly lower in this group of patients with SCD. Table 1.
- Weak correlation between PVI (%) and SpHb (g/dl), r = 0.048, p=0.54 and PI (%) 0.36, p<0.001).
- Mean (SD) SpHb concentration (11.10 ± 1.43 g/dL) was consistently higher than mean (SD) laboratory Hb (10.27 ± 1.73 g/dL) (p<0.001, with a range of bias 0.82 [-1.2 to 3.1 at n-0.2). In contrast to healthy counterparts with normal hemoglobin. Figure 4

Table 1. Demographics and laboratory data

Figure 2. correlation between spectrophotometric haemoglobin (SpHb, g/dl) and laboratory haemoglobin (Hb, g/dl).

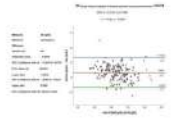

Figure 3. Agreement between spectrophotometric haemoglobin (SpHb, g/dL) and laboratory haemoglobin (Hb, g/dL)

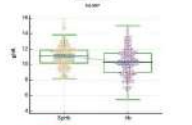

Figure 4. SpHb overestimated the Lab Hb. Inter plot with crosswiring from the median and 95% confidence interval (CI) of both (SpHb, g/dl) and (Hb, g/dL)

Conclusion

- SpHb moderately correlated with laboratory Hb and both agreed with a good degree of reliability, but with a range of bias.
- SpHb consistently higher than laboratory Hb concentrations and PI results were significantly low, in contrast to healthy counterparts with normal hemoglobin.
- More investigations among a larger population still needed to confirm the effect of PVI changes on measured SpHb concentrations.
- The effect of the low PI among SCD on the measured SpHb readings among this specific group of patients should be the focus for future research.

References

1. Weber FL, Hamelin A, Rosner MH. Continuous Noninvasive Hemoglobin Monitoring: A Diagnostic Evaluation in an Urban Hospital. Anesth Analg. 2016 Feb;122(2):367-72. doi: 10.1213/ANE.0000000000001051. PMID: 27018931; PMCID: PMC4718444.
2. Macknet MR, Allard MF, Applegate RL 2nd, Stuth E. The accuracy of noninvasive and continuous total hemoglobin measurement by pulse CO-oximetry in human subjects undergoing major surgery. Anesth Analg. 2010 Dec;111(6):1438-44. doi: 10.1213/ANE.0b013e3181f9a0ab. Epub 2010 Nov 1. PMID: 21045241.
3. Kraitl J, Ewald H, Timmer A, Lehnert H. Optical Noninvasive Determination of Total Hemoglobin Concentration in Human Subjects Undergoing Hemodialysis. Sensors (Basel). 2010;10(1):1-19. doi: 10.3390/s100100001. Epub 2010 Jan 4. PMID: 22315526; PMCID: PMC3270830.
4. Al-Mulhim HK, Al-Hathlan A, Alsaeed E, Al-Shamsi M, Al-Dayni AS, Al-Jeraisy M, Owaidah T. Validation of the Masimo Hemoglobin Evaluation in Patients with Sickle Cell Disease. Blood 2015;126 (23): 4779. doi: https://doi.org/10.1182/blood.V126.23.4779.4779.
5. Hedayati S, Bak A, Dinsio K, Gangaram-Panday N, Gupta C, Sahu S, Kanakasabai S, Bird J, Muralidharan K. Point-of-Care Hemoglobin Measurement Predicts Anemia Prevalence in Thalassemia Patients. Diagnostics. 2021; 11(1):46. https://doi.org/10.3390/diagnostics11010046

Future Scholars Program 2023

برنامج علماء المستقبل 2023

Novel nanohybrids of nickel and cobalt nanoparticles @carboxymethyl cellulose core-shell for urea fuel cell

Student Name: Fatimah Alboali

Supervisors: Dr. Hany M. Abd El-Lateef, Dr. M. Gouda

Chemistry Department, College of Science, King Faisal University

USA patent, Filing Confirmation No. 2626

Green chemistry and sustainable development track

Inventor(s): HANY MOHAMED ABO EL-LATEEF AHMED, AL-AHSA, SAUDI ARABIA; MOHAMMED GOUDA, AL-AHSA, SAUDI ARABIA; MAKMUDSTAFA HIYALAF ALI, AL-AHSA, SAUDI ARABIA; FATIMAH ABDRABBA ABDSSALMAN, AL-AHSA, SAUDI ARABIA

Applicant(s): KING FAISAL UNIVERSITY, AL-AHSA, SAUDI ARABIA

Power of Attorney: The patent practitioners associated with Customer Number: 87833

Problem

Methodology

Materials | Preparing | Casting

Results and Discussion

Objectives

Scientific Background

Graphs and Data Analysis

Materials Characterization | Electrochemical Comparison

Conclusion

Applications

Future Work

Hypothesis

Variables

References

Future Scholars Program 2023

برنامج علماء المستقبل 2023

Wireless Power Transmission of Solar Energy from Space

Mariam Almohish

Dr Mohammed AlAqil

Paper

Renewable Energy Track

Abstract

Space Solar Power (SSP), combined with Wireless Power Transmission (WPT), offers the far-term potential to solve major energy problems on Earth. In the long term, we aspire to beam energy to Earth from geostationary Earth orbit (GEO), or even further distances in space. In the near term, we can beam power over more moderate distances but still stretch the limits of today's technology. In recent studies, a 100 kWe-class "Power Pkg" satellite and a 10 MWe-class Lunar Polar Solar Power outpost have been considered as the first steps in using these WPT options for GEO. Our current assessments include consideration of orbits, wavelengths, and structural designs to meet commercial, civilian government, and military needs. National transmitter and receiver sizes are considered for power supply to a smart city on Earth. In the longer term, lunar or asteroidal material can be used. By using SSP and WPT technology for near-term missions, we gain the experience needed for sound decisions in designing and developing larger systems to send power from space to Earth.

Solar energy from space is the next frontier of energy harvesting. But how do we get the energy from space back down to Earth?

The concept of harvesting solar energy from space using an SSP (Space Solar Power System) is one of the critical methods. One of the major challenges associated with this technology is the ability to transport collected energy to Earth.

In this project, there are two major viable methods of space-to-Earth power transmission considered: Lasers, Microwaves. Hybrid

Research Aims

This research aims to transfer solar energy from space to Earth at • the lowest costs and the strongest capabilities to benefit from it

more than before

The possibility of directing solar energy relatively quickly directly to the most needed area

Removing the largest amount of greenhouse gases from the atmosphere and achieving sustainability

Materials and Methods

In the laser beam wireless power transmission technique, a laser beam source concentrated light in a photovoltaic cell receiver through the vacuum of space and the atmosphere. The receiver converts the energy back into electricity through these steps:

1. The DC power transmitted in space is used to generate a single wavelength monochromatic light beam.

2. A set of optics shapes the laser light according to the required beam size.

3. A control system ensures that the beam is pointed at the intended receiver site on Earth.

The mode of operation of the photovoltaic receiver is similar to that of solar power harvesting in which the sunlight falling on solar cells produces electricity. However, the method uses high-intensity laser beams on specialized photovoltaic cells and allows for higher efficiency than what is currently possible with solar cells. Mirrors and telescopes can be used to aim the laser beam at any receiver directly below the satellite with an unobstructed line of sight transmission path.

Materials and Methods2

We did a prototype of the shape of transmitter in space to replace with the same design of satellites with the addition of solar panels receiving solar beam side of the Earth to see how the energy is available throughout the year. The satellite consists of 3 sensors that lights the sun. 2 solar panel to transfer laser from the cube energy to the 3 laser.

To receive energy in the ground we used An dot a microscope to see our first hypothesis glass in a reflector and also a dark tube until the solar panel dispersed with the source of energy. We managed to disperse the laser light until each cell arrived, which stimulates the work of the solar panel. We observed an estimated 3.4Volt energy, which proves that the laser can be used to transfer energy to the Earth.

We did a microscope to look at the laser beam glass in a reflector and also a dark tube and the solar panel dispersed with the source of energy. We managed to disperse the laser light until each cell arrived, which stimulates the work of the solar panel. We observed an estimated 3.4Volt energy, which proves that the laser can be used to transfer energy to the Earth.

After the success of our experiment, we implemented it on the smart city to extend the city with a fully renewable energy source by stimulating the Earth's space environment.

We put a laser that represents the light coming from space and also the work of a tube as a receiver and Tesla connecting it to the whole city so that it works on a renewable energy source.

The way to move the energy is that the laser crosses through the tube that has a solar panel and then transfers the energy to the battery that in turn transfers it to the regulator that arranges the process the energy

Safety and Insurance

We know that lasers have a lot of damage, so we have to use it wisely. Laser radiation is not good and is to reduce the hazard we put the many ways within the city. We used warning signs, warning in which people can enter the dangerous fields, same may not what will happen as the same of energy or waves.

We have laws that do not provide the city with a solar panel that is for the storage and use to such benefits, some people might take advantage on the possibility of being close to the source of energy. In fact, a simple trade was done on the subject and in Multinational acquisition not violating 10%. The trade is that the laser has a high risk of deviation that could lead to loss of lights.

Results

The laser beam and microwave power transmission systems are currently the most promising technologies for wirelessly transmitting power over a long distance from a satellite in orbit to the surface of the Earth. The two methods differ in size, mode of operation, efficiency, and cost.

- The combination of ambient sunlight plus laser illumination conditions, at the terrestrial PV array, to match the daily electricity demand pattern.
- Laser light is transmitted and converted more efficiently than sun-light
  - Wavelength is selected for good atmospheric transmissivity
  - Efficient Light-Emitting Diode wavelengths match common PV band-gaps

Sustainable development

In the future, we expect power to be transferred from space directly without the need for transformers or wires, making it easier for solar energy to reach directly to homes, factories and other buildings.

Discussions

Safety of Wireless Power Transmission

In the proposed designs, the laser beams will operate at visible and near-visible wavelengths, with intensity comparable to normal sun exposure, and the intensity of the microwave radiation will be about one-tenth of that of room sunlight. Operating at these levels ensures that either transmission mode will be safe for humans, animals, and plants.

Space Solar Power Transmission

The laser beam and microwave power transmission systems are currently the most promising technologies for wirelessly transmitting power over the long distance from a satellite in orbit to the surface of the Earth. The two methods differ in size, mode of operation, efficiency, and cost.

Advantages of Laser Beam Transmission

- Does not interfere with TV, radio, Wi-Fi, cell phone and other communication signals.
- Requires smaller transmission and receiving equipment compared to microwave transmission. (For example, a 1GW installation would require about a one-meter diameter transmitting optics and a ground receiver of several hundred meters across.)

Disadvantages of Laser Beam Power Transmission

- Suffers from atmospheric absorption due to environmental factors such as rain and clouds and hence cannot provide continuous power
- Has a low conversion efficiency
- May require huge battery storage systems on the ground
- Carries the risk of causing skin and eye damage if not well managed

Laser–Microwave Hybrid Wireless Power Transmission System

- Each wireless power transmission method, microwave and laser-based, has advantages and disadvantages.
- In an effort to devise an optimal system, some researchers have considered a hybrid approach.
- A laser would transmit power from a solar array to an in-orbit base station (a solution zone) platform in such a system.
- The base station would convert energy from the laser into electricity and then into microwave radiation, which is transmitted to the receiver station on Earth.
- Thus, the laser beam is used where it does not experience significant attenuation from the atmosphere, then transmission changes to a microwave radiation, which is much less subject to atmospheric attenuation.

Conclusion

- Farther-term microwave WPT options are efficient, and can beam power through clouds / light rain, but require large sizes for long-distance WPT and a specialized receiver.
- Nearer-term Laser-Photovoltaic WPT options are less efficient but allow synergistic use of the same photovoltaic receiver for both terrestrial solar power and SSP.
- The proposed technology can enable advanced space science and exploration in the near term.
- It is hoped to have a commercial space-solar-power system operational in the upcoming 20 years.
- The technological and economic challenges facing space solar power are far from trivial.

References

[1] P.E.Glaser,"Power from the sun: Its future," Science, vol.162,pp.857–861, 1968.

[2] "Satellite power system: concept development and evaluation program," DOE/NASA, Washington, DC, USA, Rep. DOE/ER-0023, 1978.

[3] J. C. Mankins, "A technical overview of the "SunTower" solar power satellite concept," Acta Astronaut., vol. 90, no. 1, pp. 109–117, 2012.

[4] M. Nahavi, M. Klinker, M. Leipold, and A. Hansson, "European sail tower SPS concept," Acta Astronaut., vol. 69, nos. 9–12, pp. 785–795, 2011.

[5] S.Kanev, C. (2022). Could solar panels in space supply Earth with clean energy? Nature

Future Scholars Program 2023

برنامج علماء المستقبل 2023

Enhancing the Stability of Chitosan Films for Biomedical Applications through Incorporation of Tungsten, Magnesium, and Graphene Oxides

Student Name Abdullah Murtadha Alkars

Supervisors :Dr. M. Gouda, Dr. Hany Abd El-lateef

Chemistry Department, College of Science, King Faisal University

Paper, Under review

Green chemistry and sustainable development track

Abstract

Chronic bacterial infections in wounds present a significant challenge to healthcare as they hinder healing and cause various complications. This study successfully prepared a chitosan (CS) nano-frame loaded with tungsten oxide (WO3), magnesium oxide (MgO), and graphene oxide (GO) using an inexpensive polymer casting method for wound healing applications. X-ray powder diffraction (XRD), Fourier transform infrared spectroscopy (FTIR), and thermogravimetric analysis (TGA) were used to characterize the composites, and the morphology and microstructure of the film samples were examined using scanning electron microscopy (SEM). The WO3/MgO@CS composite showed a significant enhancement in UV-Vis analysis, with an intense peak at 403 nm and a narrow band gap (3.68 eV) compared to pure CS. The enhanced electron-hole pair separation rate was responsible for the WO3/MgO@GO@CS scaffold's antibacterial activity. The scaffold's ability to inhibit bacteria was tested against E. coli and S. aureus and the fourth sample showed an inhibition zone of 11.5±0.5 mm and 13.5±0.5 mm, respectively. These results demonstrate the enormous potential of WO3/MgO@GO@CS membranes as wound dressings in the clinical management of bacterially infected wounds.

Introduction

Over the past few decades, many materials for healing wounds have been employed to reduce the burden of wounds worldwide [1]. One of the main issues that endanger people's health is wound healing. Wound care raises risks and consequences because of comorbidities such as infections or diabetes [2]. Inflammation, cellular proliferation, attachment, monocyte localization, and ECM (extracellular matrix) remodeling are all involved in the wound-healing process [3]. Chronically, the wound is divided into acute and chronic cases. According to cross-sectional research in Singapore, the number of wound episodes per 1,000 patient admissions increased by 95.4% from 2013 to 2017 [4]. The prevalence of acute and chronic wounds is rising, placing a significant burden on the healthcare system. According to NHS data, between 2012 and 2018, the projected average cost per cured and unhealed wound grew by about 20.8% and 73.98%, respectively [10].

Materials and Methods

Synthesis of composites (solvent casting method):

Firstly, WO3 and MgO NPs were used as they were obtained. Graphene oxide is ready to Dennnet's method [33]. A graphite powder in 3 g was included in a 9:1 blend of concentrated H2SO4/H3PO4 under stirring for 5 min taken after by including 18 g of KMnO4 in the previous mixture with persistent stirring for 12 h. At that point, 5 mL of H2O2 was added and mixed for 1 h. The solution was washed with 30% HCl, then with distilled water, and finally with ethanol, then it was dried in the furnace.

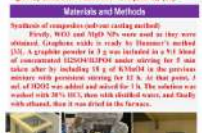

Results and Discussions

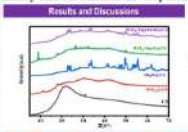

Fig. 1: XRD patterns of pristine chitosan and WO3, MgO, WO3/MgO, WO3/MgO/GO nanocomposite powder materials loaded in CS membrane (CS, WO3@CS, MgO@CS, WO3/MgO@CS, WO3/MgO@GO@CS)

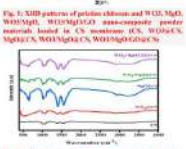

Fig. 2: FTIR spectra of the nanocomposites based on CS membrane containing WO3, MgO, WO3/MgO, and WO3/MgO/GO.

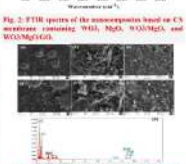

Fig. 3: SEM image of (a, a1) CS and (b, b1) WO3/MgO@CS, (c, c1) WO3/MgO@GO@CS and EDX chart of WO3/MgO@GO@CS composite (d)

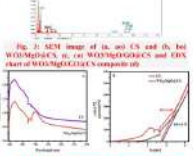

Fig. 4: (a) UV-Vis spectra of the synthesized CS and WO3/MgO@CS, (b) their energy band gap calculations from UV-Vis spectra data.

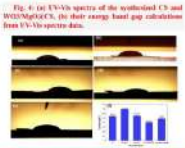

Fig. 5: Hydrophilicity of contact angle are the compositional changes, the values are 54.2 o, 40.8 o, 58.3 o, and 48.2 o for (a) CS, (b) WO3@CS, (c) MgO@CS, , (d) WO3/MgO@CS, and (e) WO3/MgO@GO@CS, respectively and (f) the contact angle of pure CS membrane and CS membrane loaded with WO3, MgO, WO3/MgO, WO3/MgO@GO.

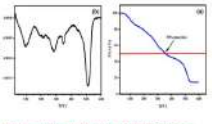

Fig. 6: (a) DTA and (b) TGA of WO3/MgO/GO@CS composite from room temperature up to 600 C.

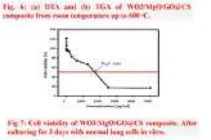

Fig. 7: Cell viability of WO3/MgO/GO@CS composite. After culturing for 3 days with normal lung cells in vitro.

Fig. 8: The antibacterial activity for all scaffolds against (a) E. coli, and (b) S. aureus.

Conclusion

A chitosan (CS) microporous membrane incorporated with WO3, MgO nanoparticles, and GO nanosheets specially prepared by non-friendly and efficient casting poly mer method or dressing for microbially contaminated wounds. FTIR, XRD, XPS, and SEM-EDS studies confirmed its incorporation. Compared to pure CS, the fabricated WO3/MgO@GO@CS composites show a significant enhancement in cell viability, reaching (121 %) Also, contact angle measurements show a great improvement in hy-drophilicity with the addition of WO3, MgO NPs, and GO nanosheets. According to TGA studies, the thermal stability of chitosan films is also significantly enhanced. By adding WO3 and MgO NPs, the degradation temperature of pure chitosan film changed to higher temperatures by 10% at 50% mass loss. The combination of MgO/WO3@GO@CS has shown a high antibacterial activity with an inhibition zone of 11.5±0.5 mm against E. coli and 13.5±0.5 mm against S. aureus. Overall, the WO3/MgO@GO@CS membrane with improved Physico-chemical characteristics has significant potential in treating wound infection and could be a good substitute for present wound dressings.

References

[1] M. Gouda, M.M. Khalaf, A. Elmarhoumi, H.F. Abou Taleb, H.M. Abd El-Lateef, Electrolyte activation of Sm2O3: Sb2O5/graphene oxide loaded cellulose acetate film, Journal of Materials Research and Technology 21 (2022) 4819–4827.

[2] R.A. Alshgari, M.M. Khalaf, M. Gouda, A. Elmarhoumi, M.F. Abou Taleb, H.M. Abd El-Lateef, Wound dressing candidate materials based on cerium films of cellulose acetate modified with zirconium oxide (ZrO2) and graften oxide (GnO2), Materials Today Communications 34 (2023) 105390.

Future Scholars Program 2023

برنامج علماء المستقبل 2023

Energy Strategy to Empower Smart Renewable Cities (SRCs)

Mariam Almuhaish, Haneen AlHassan, Rand AlMahboob

Dr Mohammed AlAqil

Paper

Renewable Energy Track

Abstract

Smart cities are an innovative concept for managing metropolitan areas to increase their residents' sustainability and quality of life. This project examines the management and evolution of energy generation, storage systems and the applications they serve, and infrastructure technology's current condition and future prospects. Additionally, the project examines energy-related construction and transportation systems and technologies. To keep a system working well throughout the year, fixed fuels must be utilized as a backup energy source. Technologies can only benefit if integrated into the city's infrastructure. By 2050, it is anticipated that the global population will surpass 10 billion, with most people settling in metropolitan regions. Between 2020 and 2027, the global market for smart energy is anticipated to expand by 27.1% annually, from USD 122.2 billion in 2020 to USD 652 billion in 2026. In 2020, Europe will account for 31.8 per cent of total smart energy product sales. China's GDP is projected to grow by 30.0 per cent annually, reaching USD 175.1 billion by the conclusion of the analysis period. Consequently, smart cities are expanding and blooming worldwide, yet there are no permanent standards.

Introduction

Smart cities are an innovative idea for managing metropolitan areas to improve sustainability and citizens' standard of living. Electronic, property, building, digitalization and smart cities are also supposed to add value to increase ecological and economic sustainability. However, the added value may be stated more straightforwardly by first addressing the benefits from the efforts.

Smart cities must address the issue of connecting their infrastructure with cutting-edge technologies that use energy efficiently and have a minimal environmental impact. Creating "smart buildings" and a more efficient transportation system is crucial in the fight against climate change and other environmental issues. As part of a smart city's balanced energy ecosystem, a well-managed automated system that can convert electric power into a limited product with minimal human intervention is required.

A single system encoding various energy, heat, gas and water networks, as well as telecommunications structures, is being developed in smart cities to balance power output and consumption, meet customer capacity, and afford other energy market participants. Electrification, the process of converting society to using electricity as the principal energy source, is essential in the long-term health of the energy sector.

Materials and Methods

This project applies a Stronglight framework to the Biggest, Purest, and Greenfield SRCs and involves identifying how the deployment of renewables contributes to smart city goals as seen in Figure 1.

•SRCs can be defined as cities with a vision that integrates renewables and smart initiatives. To qualify as an SRC, the proposed model requires that cities have a publicly available city plan that presents a vision. In addition, it must have already deployed solar and/or wind power (at least 1% of its city energy mix) and plan to deploy more.

•If the current watermill power share of the energy mix is less than 10%, the city must also have a renewable energy or decarbonization target (note that some of these targets may involve renewables other than wind and solar, and in the case of decarbonization targets, nonrenewable energy sources such as nuclear power).

Results

Three types of Smart Renewable Cities

The Biggest SRCs comprise all the cities that qualify as SRCs and have over a million residents (and many more nonresidents served).

The Purest SRCs picks up where the Biggest SRCs leave off. It includes all the cities, regardless of size, where solar and/or wind account for over 42.3% of the current energy mix.

The Newest SRCs are greenfield smart city projects entirely powered with renewables.

Discussions

- SRCs recognize that solar and wind resources play a key role in powering current city plans. This project developed the SRC framework to identify and diversify cities globally that are deploying solar and/or wind power in connection with their smart city plans.
- SRCs are the vanguard, charting a course that all smart cities are expected to pursue as they advance toward people-centered goals. While solar and wind already a part of their energy mix SRCs are strategically positioned to leverage their shared interest in renewables with utilities to more quickly achieve these goals.
- The SRC model considers the Biggest, Purest, and Newest SRCs to showcase the range of initiatives that are being implemented or considered, and the range of ways that utilities can play in initiating, shaping, or participating in them in conjunction with other service and technology providers (Figure 1.)
- Smart city plans are typically associated with the Biggest cities, which tend to be replete with legacy infrastructure and complexity, and face some of the greatest challenges and opportunities across all areas.
- Meanwhile, the Purest cities show what initiatives can bring cities closest to being primarily powered by solar and wind.
- We will use the new system provider to Hind My And to generate electricity on the roofs of buildings, which combines a wind turbine and two solar photovoltaic panels.

- Finally, the Newest greenfield projects demonstrate what a fully electrified and decarbonized deployment of SRC initiatives can potentially accomplish at various scales.
- Looking at the challenges and successes of the cities in each of these categories can help other cities and utilities determine their strategies.

Introduction

Smart cities are an innovative idea for managing metropolitan areas to improve sustainability and citizens' standard of living. Electronic, property, building, digitalization and smart cities are also supposed to add value to increase ecological and economic sustainability. However, the added value may be stated more straightforwardly by first addressing the benefits from the efforts.

Smart cities must address the issue of connecting their infrastructure with cutting-edge technologies that use energy efficiently and have a minimal environmental impact. Creating "smart buildings" and a more efficient transportation system is crucial in the fight against climate change and other environmental issues. As part of a smart city's balanced energy ecosystem, a well-managed automated system that can convert electric power into a limited product with minimal human intervention is required.

A single system encoding various energy, heat, gas and water networks, as well as telecommunications structures, is being developed in smart cities to balance power output and consumption, meet customer capacity, and afford other energy market participants. Electrification, the process of converting society to using electricity as the principal energy source, is essential in the long-term health of the energy sector.

Discussions

- SRCs recognize that solar and wind resources play a key role in powering current city plans. This project developed the SRC framework to identify and diversify cities globally that are deploying solar and/or wind power in connection with their smart city plans.
- SRCs are the vanguard, charting a course that all smart cities are expected to pursue as they advance toward people-centered goals. While solar and wind already a part of their energy mix SRCs are strategically positioned to leverage their shared interest in renewables with utilities to more quickly achieve these goals.
- The SRC model considers the Biggest, Purest, and Newest SRCs to showcase the range of initiatives that are being implemented or considered, and the range of ways that utilities can play in initiating, shaping, or participating in them in conjunction with other service and technology providers (Figure 1.)
- Smart city plans are typically associated with the Biggest cities, which tend to be replete with legacy infrastructure and complexity, and face some of the greatest challenges and opportunities across all areas.
- Meanwhile, the Purest cities show what initiatives can bring cities closest to being primarily powered by solar and wind.
- We will use the new system provider to Hind My And to generate electricity on the roofs of buildings, which combines a wind turbine and two solar photovoltaic panels.

- Finally, the Newest greenfield projects demonstrate what a fully electrified and decarbonized deployment of SRC initiatives can potentially accomplish at various scales.
- Looking at the challenges and successes of the cities in each of these categories can help other cities and utilities determine their strategies.

Results

Three types of Smart Renewable Cities

The Biggest SRCs comprise all the cities that qualify as SRCs and have over a million residents (and many more nonresidents served).

The Purest SRCs picks up where the Biggest SRCs leave off. It includes all the cities, regardless of size, where solar and/or wind account for over 42.3% of the current energy mix.

The Newest SRCs are greenfield smart city projects entirely powered with renewables.

Conclusion

- Smart cities have a growing opportunity and imperative to become SRCs.
- The integration of more solar and wind power into city energy mixes can already power their grids to be more economically competitive, sustainable, and livable.
- Utilities play a key role in their successful deployment as electrification powered by both utility-scale and distributed renewable energy spreads in the building and transportation sectors, unlocking new possibilities for customer engagement.
- The Purest SRCs have already forged the pathway, presenting smart cities as a component of their renewable energy plans, recognizing that renewable power is a starting point for smart cities.

References

Sabrut, N. 2021. How can wind and solar energy be used to configu. Kuat Renewable Energy Systems

Future Scholars Program 2023

برنامج علماء المستقبل 2023

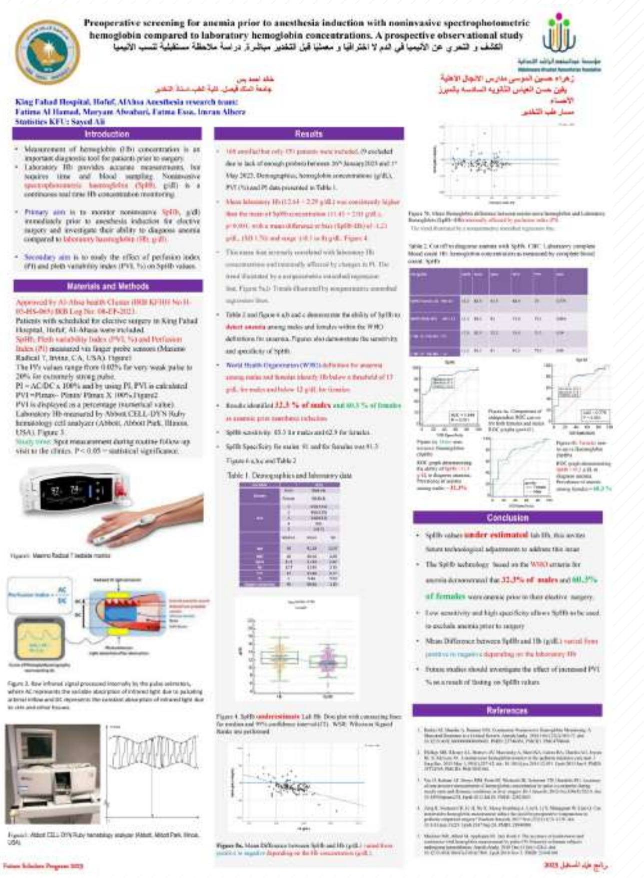
Preoperative screening for anemia prior to anesthesia induction with noninvasive spectrophotometric hemoglobin compared to laboratory hemoglobin concentrations. A prospective observational study
King Fahad Hospital, Hofuf, AlAhsa Anesthesia research team:
Introduction
Results
Materials and Methods
Conclusion
References
Future Scholars Program 2023

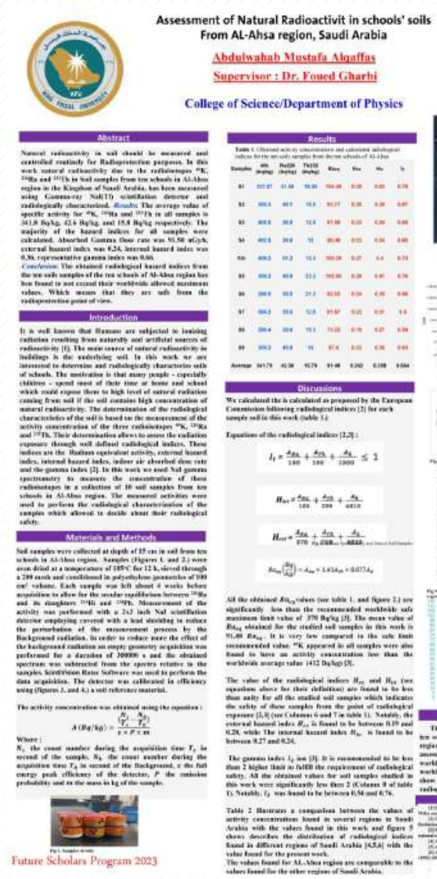
Assessment of Natural Radioactivit in schools' soils From AL-Ahsa region, Saudi Arabia
Abdulwahab Mustafa Algaffas
Supervisor : Dr. Foued Gharbi
College of Science/Department of Physics
Abstract
Introduction
Materials and Methods
Results
Discussions
Conclusion
References
Future Scholars Program 2023
برنامج علماء المستقبل 2023

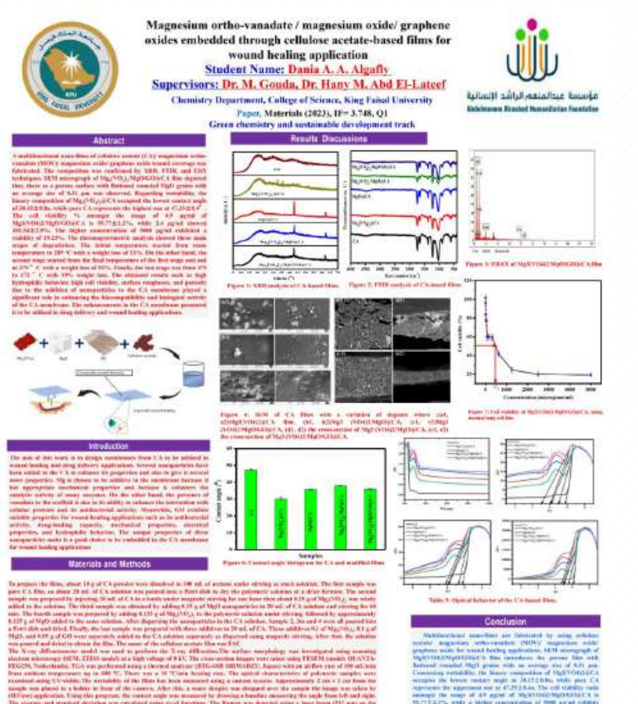
Magnesium ortho-vanadate / magnesium oxide/ graphene oxides embedded through cellulose acetate-based films for wound healing application
Student Name: Dania A. A. Algafly
Supervisors: Dr. M. Gouda, Dr. Hany M. Abd El-Lateef
Chemistry Department, College of Science, King Faisal University
Paper, Materials (2023), IF= 3.748, Q1
Green chemistry and sustainable development track
Abstract
Results Discussions
Introduction
Materials and Methods
Conclusion
References
Future Scholars Program 2023
برنامج علماء المستقبل 2023

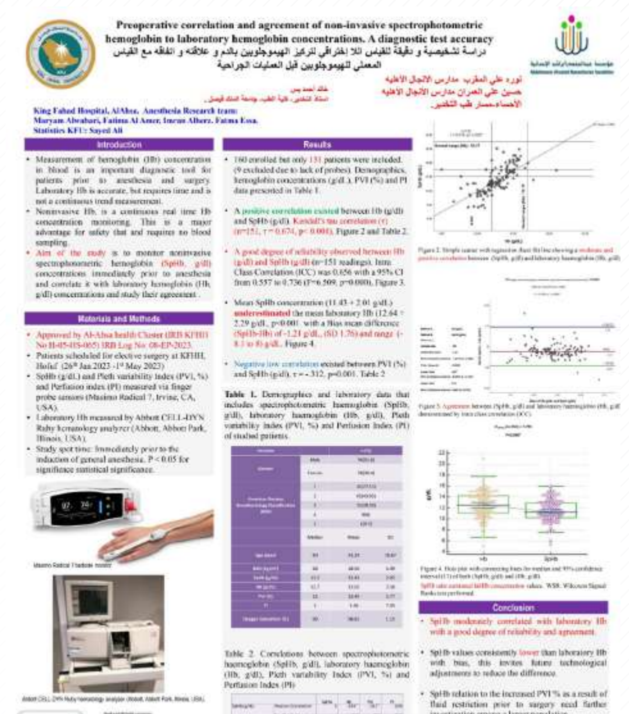
Preoperative correlation and agreement of non-invasive spectrophotometric hemoglobin to laboratory hemoglobin concentrations. A diagnostic test accuracy
King Fahad Hospital, AlAhsa, Anesthesia Research team:
Introduction
Results
Materials and Methods
Conclusion
References
Future Scholars Program 2023

Smart Solar PV Cleaning System to Enhance RES Reliability

Turki Aldulami, Abdullah Alsunayni
Dr Mohammed AlAqil

Paper

Renewable Energy Track

مؤسسة عبدالمنعم الراشد الإنسانية
Abdulmonem Alrashed Humanitarian Foundation

Abstract

Solar power is mainly harnessed from photovoltaic (PV) panels which are arranged in multiple arrays in a solar farm or solar system. Though, power generation from PV solar system is characterized by uncertain efficiency, mainly overthrow with high insolation prefer taken by an alternative way of generating clean energy. However, the efficiency of energy generated from PV panels is affected by the accumulation of dust, smog, birds droppings and coarse, even on one panel in an array. This condition leads to the need for regular cleaning of the surface of PV panels. Current robust based cleaning methods for photovoltaic arrays are costly in time, water and energy usage as well as cleaning in automation capabilities. To overcome this problem, a fully automatic solar panel cleaning system with electrical water is proposed. Hence, in this paper, the concept of a robot for automated cleaning of the surface of PV panel is presented. The design utilizes an efficient controller system to control the robot movement during the cleaning process. In addition, The cleaning system consists of two cleaning brushes in the form of stainless wings having opposite and supported by a water pump with a water tank for deep cleaning that can be used to wash dust or bird droppings found on PV panel surface. The efficiency of the PV panels before and after the cleaning process is also measured. The result shows that the developed solar panel cleaning robot is able to clean the panel efficiency and increase both the output current as well as the maximum power of the panel to 90% after the dust on the PV panel is cleaned.

Introduction

In these years, as it is known, insolation and people tend to pour more of their efforts into supporting renewable energies, in support of the environment because of solar power global warming, as the world is turning to several types of renewable energy, including solar energy.

Which prompted us to evaluate the causes of low solar energy efficiency and the conditions that negatively affect efficiency and try to solve them with a new invention of our innovation.

Some physical conditions strongly affect the efficiency of solar panels, leading to a decrease in productivity. One of these conditions is the dust effect caused by solar dusting. The existence of dust on the surface of solar panels makes a big impact on output power. Also, one of the biggest technical challenges of the solar panel is the accumulation of dirt, droppings, and bird droppings, and how severe the losses are. These factors have also negatively affect the solar panel.

Materials and Methods

The proposed solar panel cleaning robot (PSCR) comprises a microcontroller unit, battery, electronic circuit, four-wheel drive (4WD) car chassis with DC motor, water pump, water tank, and brushes. The major task of this project is to develop a robot that can automatically and controls the movement of the DC motor based on the input given by the ultrasonic sensor. It also determines the kind of cleaning action it has to perform during the cleaning process.

An ultrasonic sensor placed on the front and rear of the chassis helps the robot in obtaining distance in the form of electrical signals. Four-wheel-shaped brushes are placed on both sides of the robot and move in opposite directions for deep cleaning, in water sprays, and in water tank. Water is supplied to the brushes from the water tanks via a dedicated water pump, whose function is to pump the water at a specific pressure.

Results

The benefit of cleaning the robot is measured by several cases among in several environments and different cases, such as low humid, dust, birds droppings, and dust landing from sun-rise and together, and the result after cleaning. The efficiency of the solar panel is measured with the systems mentioned below, and it is measured under certain conditions the notice a high efficiency drop rate for some common cases such as dust, where it fell to 80%, and this is a great indication to the great value of a benefit that changes the efficiency of the solar field by continuous cleaning through the robot.

Discussions

- To test the effectiveness of the proposed solar panel cleaning robot, several experiments on cleaning a sticky solar panel were conducted. In these experiments, flour was used to imitate dust on a solar panel.
- The solar panel depends on receiving the sunlight, so anything that may block the sunlight rays will have a significant effect on the efficiency of the solar field. Therefore, the fields' efficiency is affected by various sudden weather changes such as dust and snow, and various causes such as bird droppings, tree leaves, etc. The reason that prompted us to address this problem and take it seriously is the existence of low efficiency, as it is one of the natural causes of dust, it reaches a decrease in field production by 80%.
- Therefore, focus has been placed on solving 3 main problems: Cost, manpower and cleaning efficiency, so that this robot was invented that cleans the solar panels in an automated and programmed way through the ultrasonic sensor, which allows you to smoothly program it to suit any field and any conditions.
- Also, it is worth noting that this robot has a great need in all places and is not limited to certain fields. In particular, because cleaning the panels is an essential thing from the work of the responsible company to maintain efficiency. Also, because in every geographical area there is a reason to ensure the efficiency of the fields, such as dust in desert areas, snow storms, and also the autumn season in agricultural or tropical areas, so this invention has a wide all over the world.

The most prominent feature of the robot is the cleaning system and moving brushes with opposite rotational motion at high speed, which allows it to clean clean smoothly and quickly, as well as the four-wheel drive system and high torque that allows the drone to climb despite the presence of the most difficult conditions.

The experiment performed under this category contains analysis of the impact water insolations due to dust.

The study was carried out using different values of voltage and current to make PV module with different real samples having different weights on three irradiation values of 800, 700 and 600 W/m².

A group of the data indicates the power reduction due to the accumulation of dust on the PV module. Data indicate that in the case of thickness 0.1 gm per square meter, the maximum power losses of 4% to 30 (0.3 gm) to 10% have been observed.

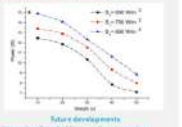

Future developments

1- Improving the robot in managing some cases:
such as the common fires that occur in the fields of solar panels.

2- total control of remote area.
Link Cell and Wi-Fi can be performed by the technician can't solve it because he is not available at this area.

3- Developing special versions for different places
, so that the capabilities are more compatible with the type of obstacles that it will meet, such as dust and snow.

Conclusion

- In this project, a fully automated solar panel cleaning robot has been developed. The control algorithm and cleaning sequence are automated with the ultrasonic platform. The robot is designed to be fully powered by rechargeable batteries. The experiment and verification results demonstrate the functionality of the cleaning robot to perform its duty.
- The solar photovoltaic output power is successfully restored to its maximum power capacity after the cleaning process, even though there are slight losses due to some pitted error in this system. The 90% improvement in the output current, as well as the maximum power before and after cleaning, reveals that the robot guarantees effectiveness of the developed robot.

References

Future Scholars Program 2023

Smart Solar PV and Wind Turbines Monitoring System

Abdullah Alsunayni , Turki Aldulami
Dr Mohammed AlAqil

Paper

Renewable Energy Track

مؤسسة عبدالمنعم الراشد الإنسانية
Abdulmonem Alrashed Humanitarian Foundation

Abstract

Smart Grid technology as a platform can encompass several advanced technological features across the spectrum of the power system. Smart Grid may introduce an expert system for structural damage on the surface of large-scale power utility facilities providing crucial information to maintain the safety of the plant. To achieve such a cost-effective structural health monitoring system, a holistic smart inspection implementation framework is required. Using recently available sophisticated inspection technologies, a high-resolution image showing the structural condition of large infrastructure can be routinely acquired as a remote monitoring process. Automated analysis of these inspection images can significantly reduce the inspection cost, provide an effective detection mechanism, and shorten reporting time, as a result, reducing overall maintenance costs, and improving safety measures. In this work, we have applied state of art deep learning-based inspection image analysis methods for surface damage detection of various renewable energy power plants with a single unified model. We have achieved the state-of-the-art accuracy in 0.76 mean average precision on average even where input images are of varied modalities from thermal images to visual images from high- to low-resolution images, and from solar panels to wind turbines. All validations have been tackled with one single deep-learning model to detect surface damage. Our results demonstrate the promise of effectively deploying a single trained model to inspect a wide range of energy installations while reducing the necessary computing resources.

Introduction

- Because one of the main assets of vision 2030 is " A Thriving Economy" using renewable energy sources is an important aspect of thriving our economy and developing our nation. A great deal of renewable energy we own are in PV solar systems that is exposed to vast climatic, that have our many construction and challenges that we have met when applying our PV systems. One of the biggest ones is the problem of inspecting the solar panels and discover any defections or problems before we decided to conduct our maintenance and replacement regarding that issue.
- For the process of inspection, there are several stages of thinking we used through, but to simplify the following:
- For PV arrays, the impact of weather is significant. Any dust, for example, can decrease the efficiency dramatically. Another thing is, with the increase in the drone use, we can monitor many of our solar panels in different types of damages in PV panels. What I believe breaks are it is depicted in my list, as well as last one, when we evaluate energy system that our crew have.
- Detecting these types of damages with drone images required an efficient and automated image processing method. Automation can decrease the required processing time and, therefore, human involvement in analyzing these media. Thorough experimentation by training deep learning-based models can evaluate the effectiveness of such a system. Making the processes of these systems is good as it is still however.

Materials and Methods

- The proposed method was tested on wind turbine blades, PV panels, demonstrating the promises of the extensibility to other large power plant maintenance Fig. 1 illustrates the proposed framework for using drone-based detection and classification. The prediction performance of power installations having a machine learning backbone using deep learning.
- The proposed framework is segmented into three major components:
  - The first part: deals with image acquisition using defensive sensor installations with drones.
  - The second part: handles machine learning to learn about damages.
  - The third part: the application applies the learning to infer the location of damages, estimate the severity based on the location and suggest possible measures to the human decision-maker.

Figure. 1

Results

The measured data is taken for three solar PV cleaning conditions:

- Before Dust
- During Dust
- After Dust

The calculated real power obtained from the measured voltage and current is provided in Figure 2 provides the current versus voltage (I-V) characteristic of the unfouled, dusty and cleaned solar panel. From the data given, the current decreased by almost 50% when the solar panel was covered by dust. The real power provided by the solar panel also decreased linearly with the reduction of the current. Then the cleaning process was done by using the developed robot. After the dust cleaning process, the current increased back almost by 50%.

Figure 2

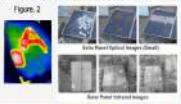

Solar Panel Optical Images (Small)

Solar Panel Infrared Images

Discussions

- Images are taken from the experiment to performed by 4K thermal cameras for monitoring the effects of the soiling, having different particle sizes and colors) on power production, regarding a control PV panel without soiling. Here the images are 160 × 192 pixels in resolution.
- This particular image set has 122 high-resolution long shots of 3264 × 1836 pixels dimension color images. These images are taken with a handheld camera and annotated as damages where PV panels are covered by dust.
- Solar Panel Infrared images are collected and annotated according to the hot spot features. In this image set, images were acquired using a 640X 4K camera with a RGBD drone. All the images in the set are 306 × 256 pixels in dimension and grayscale.
- The experimental results of this work show that, for the used optical image datasets, the performance is more sensitive to the quantity and quality of the image (considering image augmentation). One of the main reasons is that different types of damage can have considerably different appearances necessitating data sources. Then, different object detection methods need a significant number of examples to learn from.
- As a result, for the cases of the combined image dataset, the detection precision is higher compared to the smaller damage dataset. Also, one of the important considerations in selecting any deep learning architecture for object detection purposes is the amount of complexity or the hardware requirements that come with it.

- The most advanced deep learning architectures, the models can learn to recognize damages with precise bounding boxes even when the damages are from varied structures, acquired with different sensors, and possess longer ranges of shapes, sizes, viewpoints, and other external artefacts.

Figure. 3

Conclusion

- The cost of renewable energy installation maintenance for ensuring safety and enhancing production rate can be significantly reduced using automated damage detection based on routinely acquired drone inspection images, and will also increase the durability and lifetime of large power plant installations.
- This work explored four different datasets and six different dataset combinations to perform experimentation of state-of-the-art object detection architectures.

References

Future Scholars Program 2023

برنامج علماء المستقبل 2023

in vitro antibacterial activity of Thyme (*Thymus vulgaris*) against foodborne pathogens

Munthir Jafar A Aljafar
Dr. Sallah A. A. Al-Hashedi and Prof. Dr. Khaled Ramadan

Paper

Engineering and Manufacturing track

مؤسسة عبدالمنعم الراشد الإنسانية
Abdulmonem Alrashed Humanitarian Foundation

Abstract

Background and Aim: Thymus vulgaris (known as Zaatar in Arabic) is belonging to the Lamiaceae family, in Saudi Arabia Thyme is commonly used as a flavouring agent in Arabic breads, cheese pizza, pickle and in some other snacks and also used as alternative system of medicine and as a natural food preservative. This study aimed to determine the antibacterial activity (in vitro) of Thymus vulgaris essential oils against Gram positive and negative foodborne diseases bacteria and some probiotic bacteria such as Streptococcus thermophilus.

Results: Thyme essential oil has biological activity, TEO exhibited inhibitory effects toward all tested foodborne diseases or pathogens bacteria and less inhibitory effects toward all probiotic bacteria like Lactobacillus delbrueckii.

Conclusion: Thyme plays an important role in human health, TEO was examined for its antimicrobial activity to provide of its health benefits to consumers. TEO exerted potent antimicrobial activity against G. aurous, L. monocytogenes, S. Salmonella enterica and E. coli. It is concluded that the TEO has more potential to be used in the food industry as a natural antibacterial.

Keywords: Zaatar (Thymus vulgaris), essential oils, Salmonella enterica, Lab. antibacterial activity, Subgenium, well assay.

Introduction

Thyme known as Zaatar in Arabic is an aromatic evergreen shrub belonging to the Lamiaceae family. There are over 350 species of Thyme grown in many parts of the world but is more indigenous to Europe and the Mediterranean basin. Thymus vulgaris is local to the Mediterranean region and to the common species planted in Arabic world in addition to certain African countries including Egypt. Thyme in Saudi Arabia is commonly used as a flavouring agent in Arabic breads, cheese pizza, pickle and in some other snacks. It is also used in the alternative system of medicine since ancient time as a remedy for cough, toothache, bronchitis, constipation, warts, hemorrhea, alopecia, epsom, indigestion, inflammation, skin infections and for its diuretic properties (Basch et al., 2004; Khaniki et al., 2023).

The thyme leaves have medicinal properties attributed to its volatile constituents (Nasrat et al., 2020). Odorous constituents of plant oils are used as; flavoring agent in food and drug industry, starting material for the synthesis of complex medicinal compounds, therapeutics agent for skin and upper respiratory illnesses, lipophilic solubility enhancer, carrier of drugs, cosmetic and in fragrance industries (Shrivastava et al., 2010). Thyme oil has commercial importance partly because of its aroma and thus frequently added to different kinds of ointment and fillets. It is also used as a natural food preservative in food industry. It is commonly used in preparation of soaps, perfumes, beautifying products and some aromatic solutions in fragrance and cosmetic industries (Cowan&ee et al., 1999; Sokovi et al., 2006).

Materials and Methods

1. Bacteria and growth media

Bacterial strains (ATCC and DSM strain) used as indicators for thyme essential oil evaluation for *in vitro* antimicrobial activities are shown in Table (1). Lactic acid bacteria (LAB) reference strains, were propagated in MRS broth (Oxoid, UK) at 37°C ± 1° for up to 48 h and pathogenic bacteria (indicators) were activated in Brain Heart Infusion (BHI broth (Oxoid, UK) at 37°C ± 1° for 24h ±2. Working culture (LAB and other indicators) were maintained at 5°C in MRS+1.5% agar (deep agar for LAB) or slants of BHI +1.5% agar (for indicators). Prior to use each strain was activated twice in the appropriate broth and conditions and stab or steel cultures were transferred and activated bimonthly for making new working cultures.

2. *In vitro* antimicrobial activities of thyme essential oil (TEO):

In vitro antimicrobial activities for TEO were screened using the agar well assay of Rekid et al., (2016). Sterilized 100 ml Nutrient Agar (Oxoid, UK) were tempered to 48°C (water bath) prior to seeding with 100µl (10⁵ CFU/ml) of diluted culture from the indicators listed in Table (2). Inoculated media were poured into Petri plates (in replicate) then left to handles under room temperatures. Wells (6 mm in diameter) were made in the agar with a sterile Cork bore (stainless steel bores) and each well was filled with 100µl of CEO. Plates were left at room temperatures for 30 min to allow diffusion of CEO. Inhibition zones (including well diameter) around wells were measured in mm after incubation at 37° C. Clear zones greater than 6 mm were considered as active CEO against the indicator. Zones of inhibition were measured and the average zone size of each dilution was taken.

3. Kirby-Bauer technique (Disk Assay)

Susceptibility Table 3) to 6 types of antibiotics was performed by the disc diffusion method (Kirby-Bauer technique) as recommended by National Committee for Clinical Laboratory Standards (NCCLS) and as described by Khalil (2009). Commercially available antibiotics disc (Oxoid, UK) Vancomycin (5 µg) VAN, Kanamycin (30 µg) K30of the 6 reference strains isolates (, Amoxycillin (30 µg) AMC30, Tetracycline (30 µg) TE30, and Chloramphenicol (30 µg) C30, were placed on the surface of the agar plates. Liquid cultures of the 6 reference strains were incubated overnight at 37° C, and their wells were diluted by sterile peptone (0.1% w/v) to reach a count of 10⁶ CFU/ml. Sterilized 100 ml Nutrient Agar (Oxoid, UK) were tempered to 48°C (water bath) prior to seeding with 100µl (10⁶ CFU/ml) of diluted culture from the indicators listed in Figure (2). Plates were incubated (24h) at 37° C. (5 discs per plate, each in replicate plate). After incubation, the diameter of the zones of inhibition was measured.

Results

Table (5). Indicator bacteria used in the study

Bacteria	Code
Lactic Acid Bacteria (LAB)	
Lab. Salivarius strain, Subgenium	MRS/TAMU 1360
Lab. Salivarius strain, yellow strain	MRS/TAMU 1517
Streptococcus thermophilus	MRS/ATCC 19258
Pathogenic and Spoilage Bacteria	
Listeria monocytogenes	ATCC 19115
Staphylococcus aureus	ATCC 25923
Escherichia coli	ATCC 25922
Pseudomonas aeruginosa	ATCC 27853
Enterobacter aerogenes	ATCC 13048
Salmonella enterica	ATCC 13076

(*) Microorganisms with T (Type).
ATCC, American Type Culture Collection.

Table (7). Susceptibility of Foodborne bacteria to thyme essential oil (TEO) using the well assay, inhibition zone (mm).

TEO conc. (µl/ml)	Pathogenic Gram-negative bacteria				Pathogenic Gram-positive bacteria			Lactic acid bacteria (LAB)	
	Gram-negative bacteria				Gram-positive bacteria				
	SE70	P1643	EC122	8480	A.A.7	L.S.648	L.M.91	L.S.20	ST17
91	19	2.5	21	20	24	18	19	19	19
45.5	11	–	11	11	12	11	–	11	11
22.8	9	1.5	10	11	12	9.5	–	–	–
11.4	–	–	9.5	–	10	8.5	–	–	–

Refer to Table (3) (*) ... no inhibition.

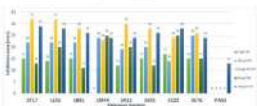

Figure (1). Sensitivity of foodborne bacteria to Clove essential oil (CEO) using the well assay, inhibition zone (mm).

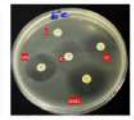

Refer (1): Zone of inhibition used for different concentration of CEO against Staphylococcus aureus (+ve) , (2,3,) using well different assay.

Figure (2). Inhibition zones (mm) for antibiotic disc, against reference bacteria.

Refer (2): Zones of inhibition caused by different antibiotic disc against Staphylococcus aureus (ATCC 25923) using disc diffusion assay.

Discussions

Taghavod et al., (2023) reported the TEO has antibacterial activities against pathogenic bacteria isolated from the hospital patients, such as *Enterococcus faecalis*, *Serratia fonticola*, *Staphylococcus aureus*, *Klebsiella pneumoniae*, *E. coli*, and *Enterobacter aerogenes* and it demonstrated a considerable antibacterial activity with minimum inhibitory concentrations (MIC) from 2 to 9 µL/mL against all strains except *Staphylococcus aureus* (MIC = 32 µL/mL), whereas the highest inhibitory effect for thyme leaves and stems essential oil was imposed on *Klebsiella*, *Escherichia coli*, and *Staphylococcus aureus*, and the largest inhibitory zone diameter of essential oil appeared against growth *Salmonella paratyphi* B (Mehrabi et al., 2021).

Conclusion

Thyme plays an important role in human health due to the presence of phytochemicals which contributes to many health benefits. In the current study, TEO was examined for its in vitro antimicrobial activity to provide a justification of its health benefits of daily consumption. TEO exerted potent antimicrobial activity against both Gram positive and negative pathogenes bacteria such as *S. aurous*, *Listeria monocytogenes*, *Salmonella enterica* and *E. coli*. It is concluded that the TEO has more potential to be used in the pharmaceutical and food industry as a natural antibacterial.

References

Future Scholars Program 2023

برنامج علماء المستقبل 2023

Manipulating stability of chitosan films by the addition of tungsten, magnesium, and graphene oxides for biomedical purposes

Student Name: Fatimah Alaithan
Supervisors : Dr. Hany M. Abd El-Lateef, Dr. M. Gouda

Paper, Under review

Chemistry Department, College of Science, King Faisal University

Green chemistry and sustainable development track

مؤسسة عبدالمنعم الراشد الإنسانية
Abdulmonem Alrashed Humanitarian Foundation

Abstract

Chronic bacterial infections can impede wound healing and lead to various complications, posing a significant challenge in healthcare. To address this issue, researchers developed a chitosan (CS) membrane loaded with tungsten oxide (WO_3), magnesium oxide (MgO), and graphene oxide (GO) for wound healing applications. The membrane was prepared using a cost-effective polymer casting method and characterized using X-ray powder diffraction (XRD), Fourier transform infrared spectroscopy (FTIR), and thermogravimetric analysis (TGA). Scanning electron microscopy (SEM) was used to examine the morphology and microstructure of the film samples. The WO_3/MgO/GCS composite exhibited a significant improvement in UV-Vis analysis, with a strong peak at 480 nm and a narrow band gap (2.69 eV) when compared to pure CS. The WO_3/MgO/GCS/GCS scaffold demonstrated antibacterial activity due to the enhanced electron-hole pair separation rate. The average cell viability of the nanocomposite scaffolds was evaluated using human lung cells, and the WO_3/MgO/GCS nanocomposite reached 121% with an IC50 value of 1454 µg/mL. The scaffold's ability to inhibit bacteria was tested against E. coli and S. aureus, with the fourth sample exhibiting an inhibition zone of 11.5±0.5 mm and 12.5±0.5 mm, respectively. These findings suggest that WO_3/MgO/GCS/GCS membranes have the potential to serve as effective wound dressings for clinically managing bacterially infected wounds.

Introduction

Over the past few decades, many materials for healing wounds have been employed to reduce the burden of wounds worldwide [1]. One of the main issues that endanger people's health is wound infection. Wound care raises costs and consequences because of comorbidities such as infections or diabetes [2]. Inflammation, cellular proliferation, attachment, remodelling, and ECM (extracellular matrix) remodeling are all involved in the wound-healing process. Clinically, the wound is divided into acute and chronic kinds. This kind of injury typically takes a healing period of around 12 weeks because of many causes, including temperature changes, healing agents, and chemical exposure. While the chronic form typically requires more time to heal because of ongoing inflammation because of some factors like physical trauma or infections. A pattern of rising wound incidence in surface care has been identified by data from multiple studies. Observational clinical trials that were carried out in numerous nations throughout the world provide proof of this. According to cohort research conducted in the UK, the National Health Service (NHS) had a 71% increase in wound incidence between 2012 and 2018.

The loaded nanoparticles in the membrane should be safe and non-toxic for the human body. Different studies have reported several concentrations of nanoparticles for the healing process. J. Prabakti et al. fabricated a collagen acetate nanofiber membrane encapsulated with GO/TiO2/Curcumin. The authors have used 5 g of the composition in the fabricated nanofiber scaffold. On the other hand, H. Razi et al. fabricated a nanofiber scaffold for wound dressing applications. About 1% of TiO2 was added to the blend to fabricate the scaffold. So, the use of concentration in our work is thought to be safe for the human body.

So far, few researchers have reported composites combining CS and WO_3, MgO NPs, and GO nanosheets. Based on this concept, novel WO_3/MgO/GCS/GCS composite membranes were successfully prepared via an easy, inexpensive polymer casting method in this paper, and their wound healing efficiency was also investigated.

Materials and Methods

Firstly,WO_3 and MgO NPs were used as they were obtained. Graphene oxide is ready by Hummer's method [33]. A graphite powder in 1 g was included in a 9:1 blend of concentrated H_2SO_4/H_3PO_4 under stirring for 1 min taken after by including 18 g of KMnO4 in the previous mixture with persistent stirring for 12 h. At that point, 3 mL of H_2O_2 was added and mixed for 1 h. The solution was washed with 30% HCl, then with distilled water, and finally with ethanol, then it was dried in the furnace.

Results &Discussions

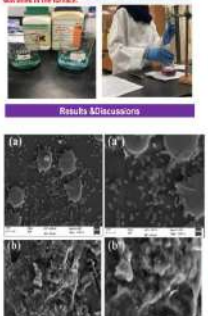

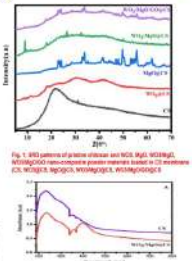

Fig. 1. XRD patterns of pristine chitosan and WO_3, MgO, WO_3/MgO, WO_3/MgO/GO nano-composite powder materials loaded in CS membrane (CS, WO_3/CS, MgO/CS, WO_3/MgO/CS, WO_3/MgO/GO/CS).

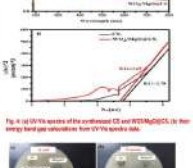

Fig. 4. (a) UV-Vis spectra of the synthesized CS and WO_3/MgO/GCS, (b) their energy band gap calculations from UV-Vis spectra data.

Fig. 5 The antibacterial activity for all scaffolds against (a) E. coli, and (b) S. aureus.

Introduction

Conclusion

A chitosan (CS) nanocomposite membrane incorporated with WO_3, MgO nanoparticles, and GO nanosheets specially prepared by eco-friendly and efficient casting polymer method or dressing for microbially contaminated wounds. The WO_3/MgO/GCS/GCS membrane showed its incorporation. Compared to the pure CS, the fabricated WO_3/MgO/GCS/GCS composites show a significant enhancement in cell viability, reaching (120 %). Also, contact angle measurements show a good hydrophilic nature in the hydrophobicity with the addition of WO_3, MgO NPs, and GO nanosheets. According to TGA studies, the thermal stability of chitosan films is also significantly enhanced. By adding WO_3 and MgO NPs, the degradation temperatures of pure chitosan film changed to higher temperatures by 11% at 30% mass loss. The combination of WO_3/MgO/GCS has shown a high and dose-wise activity with an inhibition zone of 11.5±0.5 mm against E. coli and 12.5±0.5 mm against S. aureus. Overall, the WO_3/MgO/GCS/GCS membrane with unique physicochemical characteristics has significant potential in treating wound infections and could be a good substitute for proper wound dressings.

References

Future Scholars Program 2023

برنامج علماء المستقبل 2023

Potential probiotic characteristics of bacteria from Asfar Lake and their antimicrobial activity against bacterial pathogens

Najla Alsaud and Hela alobaidan
Dr. Ashraf Khalifa and Dr. Hairul Islam Mohamed

Paper/ Patent

Biotechnology

Abstract

A microbiota in lake environment has rich source of uncharacterized microbes. In this study three isolates; ASF-1, ASF-2 and ASF-4 from the Al-Asfar lake, Al Ahsa Lake were isolated. They were active against high pH and hydrophobic characters. The isolates were further screened for fermentation capacity of Hasawi rice. The active proteins was evaluated for antimicrobial activity. It showed potential antimicrobial components extracted from probiotic fermented

Introduction

Al Ahsa oasis of dessert has unique and beautiful lake system, has an exceptional importance at national and international levels. This water body, which once considered as divine source of water is now increasingly being abused and severely polluted. The aquatic systems are mostly dominated by bacteria and fungi and in the natural environments micro-organisms have very specific roles with regard to the recycling of materials and purification of water.

The fermentation of rice is carried out by lactic acid bacteria (LAB) like *Lactiplantibacillus plantarum Lactobacillus delbrueckii* (Piraban et al., 2020). About 100 g of fermented sour rice contains 73.91 mg iron, 839 mg potassium, 303 mg sodium and 850 mg calcium. Fermented sour rice contains an increased amount of vitamin-B complex and vitamin-K, and is also regarded as a high energy-rich and body rehydrating food.in this study, probiotic characteristics bacteria used for Hasawi rice fermentation and bio components were extracted and evaluated for antimicrobial activity and protein rice components.

Materials and Methods

Isolation of pure colonies.
The pure colonies were isolated in new plate and incubate 37° C for 48 hours.

Fermentation with Hasawi rice for 15 days
Rice (20 g) was then homogenized with 25 mL of fermentation media. The inoculum of the three probiotic strains were added separately and incubated at 37° for 24 h

Quantification of total protein.
Done using Bradford reagent.

Antibiotic sensitivity assay
Antibiotic sensitivity test was performed by the Kirby-Bauer disk diffusion test (Bauer et al., 1966)

Antibiotic discs were placed on freshly prepared lawns of each isolate on Mueller-Hinton agar (MHA) plates and incubated for 24–48 h at 37 ° C. Gentamicin (120 µg), Amikacin (30 µg), Ciprofloxacin (5 µg), Methicillin (5 µg), Streptomycin (10 µg) were studied in this study.

Antimicrobial study
Extraction of antibacterial agents and evaluation of their antagonistic activity against *Staphylococcus aureus, Salmonella typhi, S. enterica*

Results

Isolates from asfar lake fresh water

Antibiotic sensitivity assay

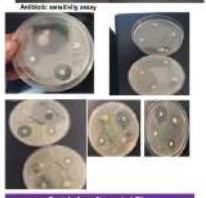

Protein from fermented Rice

Antibiotic susceptibility

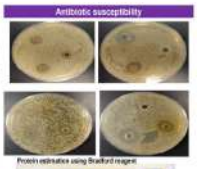

Protein estimation using Bradford reagent

Discussions

One important feature of the probiotic bacteria is their ability to secret bioactive compounds that can kill or suppress the growth of pathogenic bacteria. In this study, the two bacterial isolates from Al Asfar Lake that fulfilled the probiotic standards, displayed significant sensitivity towards certain common antibiotics including Amikacin (20 ug/disc), ampicillin, streptomycin and ciprofloxacin. The two active isolates showed sensitive against all the tested antibiotics and showed <10 mm zone of inhibition in agar plate method. The significant isolate has been selected for further fermentation of Hasawi Rice in order to assess its ability to generate unique bioactive proteins with potential therapeutic activity against inflammation. The extracted protein from probiotic-fermented Hasawi rice showed bioactivity against bacterial pathogens (*Salmonella* and *Staphylococcus aureus*.

Conclusion

Novel bioactive protein was obtained from probiotic-fermented Hasawi rice. Further In vivo study using the selected proteins was conducted in inflammation-induced mice model

References

Chahal DS, El Biaz M, Cote-Mata P, Bouabdesse A, Sarma-Velazquez J. Discovery of novel lipopeptaibiotic agents with inhibitory effects on growth of food-borne pathogens and their application to seafood products. Res Microbiol. 2012; 163(1):44-54. 10.1016/j.resmic.2011.08.006

Ghalfa A, Ghedin A, Ibrahim HM. Bacillus amyloliquefaciens Enriched Camel Milk Attenuated Colitis Symptoms in Rats Model. Nutrients. 2022; 14(9):1907. https://doi.org/10.3390/nu14091907

Future Scholars Program 2023

برنامج علماء المستقبل 2023

Validation of mass attenuation coefficient for polymethylpenten, water, cement, concrete, gypsum and brick, using Monte Carlo method with Geant 4.

Zahra Emad Alghuffy
Supervision :Dr. Foued Gharbi

College of Science/Department of Physics

Abstract

Mass attenuation coefficient, μ/ρ for several environmental materials such as polymethylpenten, water, cement, concrete, gypsum and building bricks, have been calculated using Monte Carlo simulation code (Geant4 at different gamma ray energies less than 2 MeV. The found μ/ρ values were validated by comparison with experimental and theoretical XCOM results, as well as compared to values found by other authors using Geant4 and MLNP codes. Our developed code can be used as efficient alternative to experimentation when chemical composition of the material is known.

Introduction

Mass attenuation coefficients were calculated using a developed Geant4 code [1]. Geant4 toolkit is a universal Monte Carlo code that can be used to simulate the interaction history of electrons, neutrons and photons and their coupling within a medium. With its huge cross-section database, Geant4 can simulate the interaction between these particles and energies from 1 keV to 100 MeV.

Theoretical Validation was done based on XCOM results [7]. Experimental validation was done based on published data in the literature [4, 5, 6]. The resolution of the detector was not considered in the present simulation to improve the accuracy of the simulated mass attenuation coefficients. The developed code was tested for Polymethylpenten [3] , water [4] and samples of building materials [6]. We used zero resolution in this work because simulation allows it and because a perfect detector can provide more accurate values of mass attenuation coefficients than a realistic one.

Materials and Methods

1. Geant4 :
The main classes to be implemented by the user to perform a Geant4 simulation virtual experiment are :
-*Detector Construction Class* : used to design the geometry of the virtual experiment.
-*Physics List Class* : used to instantiate the Geant4 class responsible of the simulation of the physical processes involved in the interaction of the Gama rays with media for energy less than 2 MeV. These interaction process are : Photoelectric effect, Compton Scattering and Gama Conversion.
-*Primary Generator Action Class* : used to generate primary kinematics of primary photons (energy and momenta).
-*Event Action Class* : used to score (collect) the desired information during the tracking of particles (deposited energy).

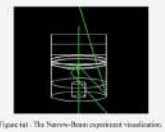

Figure (a) : The Narrow-Beam experiment visualization.

Figure (a) illustrates a visualization of the realized virtual experiment -Narrow beam Beer Lambert experiment- in action using Geant4 software, this experiment is based on Equation (1).

$$N = N0\, e^{\mu x} \quad (1)$$

N is the gamma ray counts which penetrates the sample without interaction and totally absorbed inside the detector.
N0 is the gamma ray counts totally absorbed inside the detector without the presence of the sample.
x is the thickness of the sample.

The mass attenuation coefficient μ (μ/ρ) is a key factor for evaluating the effect of gamma radiation at appropriate energy with the studied material and can be deduced from Beer-Lambert Law as follows in Equation (2)

$$\mu = \frac{-1}{x\rho} \, Ln\left(\frac{N}{N0}\right) \quad (2)$$

ρ is the density of the material

2. XCOM :
Comparison between mass attenuation coefficients for the polymer and building materials using XCOM software online and Geant4 code at various photon energies.

3. Resolution effect :
The energy resolution (Re) of a detector measures its ability to distinguish gamma-rays with close energies and the ability to distinguish between two peaks.
We did run with resolution and without resolution the developed Geant4 code (res=0), because we the resolution can affect the result.

Results

Discussions

For all the studied samples (polymethylpenten, water, gypsum, brick and cement) we found that we are closer to theoretical XCOM values than to the calculation results by other authors using Geant4 [3] , MLNP [3] (Singh) and to experimental results (Medhat).

Cement: Table lists the Mass attenuation coefficient results from Geant4, XCOM program and Medhat experiment. It is evident that calculated mass attenuation coefficients without considering the resolution of the detector provides a closer values to the theoretical XCOM ones. Relative deviation RDV (%) between (XCOM with G4 res = 0) and (XCOM with G4 res not 0) was compared using Equation (3)

$$RDV\% = \frac{(\mu/\rho)Geant4 - (\mu/\rho)XCOM}{(\mu/\rho)XCOM} \quad (3)$$

The RDV% are represented in Figure (b).
Figure (c) represents the mass attenuation coefficients. It is clear that the Geant4 calculated mass attenuation coefficients Geant4 is closer to XCOM than the experiment values [6].

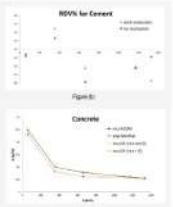

Figure (b)

Figure (c)

Conclusion

The developed Geant4 code in the present work can be a very useful alternative for the calculation of mass attenuation coefficients of the gamma ray in building materials when their chemical composition is provided. The present simulation uses the advantage of not involving the resolution of the detector in the calculation which improves its precision. The present code will be extended to other building materials and polymers (resin polymers).

References

[1] Geant4 https://geant4.web.cern.ch/

[2] XCOM: http://physics.nist.gov/PhysRefData/Xcom/Text/intro.html

[3] MCNP5 https://mcnp.lanl.gov

[4] Singh VP, Shirsath SE, M. E. Medhat Badiger NM. Determination of mass attenuation coefficient for some polymers using Monte Carlo simulation. Nuclear (2015); Jun 10 (2016) ; vol.ume 93:146-156.

[5] Abbas, H.T., Abdulsada, I.D., Jassim, M.I., Abbas, H.G., Rahman, H.I., Al-Ubaidi, A.M., Ajeel, K. Gamma-ray attenuation and Exposure Build-up factor of Some Polymers Shielding. Iraqi Journal of Science, Materials 2021 ; 62, 3455

[6] Medhat ME. Gamma-ray attenuation coefficients of some building materials available in Egypt. Ann Nucl Energy 2009; 36:189-93.

Future Scholars Program 2023

برنامج علماء المستقبل 2023

Carboxymethyl Cellulose based hydrogel decorated with Ag/Fe nanocomposite and its Electro-catalysis of 2,4-Dinitrophenol application

Student Name: Fatimah Ali Alkhalaf
Supervisors: Dr. M. Gouda, Dr. Hany M. Abd El-Lateef
Chemistry Department, College of Science, King Faisal University

USA patent, Filing Confirmation No. 9501

Green chemistry and sustainable development track

Abstract

The growth and reproduction of animals and plants, as well as the survival and development of humans and the environment, are all seriously threatened by low-concentration organic dye effluent. Due to their superior adsorption performance, flexible hydrogel composites have been created; nonetheless, the high removal efficiency and quick adsorption rate remain two major issues with regard to practical applications. The produced Ag nanoparticles-doped-Fe nanoparticles were encased in carboxymethyl cellulose (CMC/Ag-Fe). The optical, structural, morphological, properties of CMC/Ag-Fe nanohybrid materials were thoroughly characterized using FESEM, and XRD. Using a glassy carbon electrode (GCE) embellished with a wet-chemically produced CMC/Ag-Fe electro-catalyst, differential pulse voltammetry (DPV) was used to investigate the electrochemical oxidation-reduction research of 2,4-dinitrophenol (2,4-DNP). A potential method for the effective oxidation and reduction of contaminants from industrial effluents is therefore offered by the developed catalyst.

Introduction

In recent years, water contamination has grown to be a serious issue [1]. Additionally, the US Environmental Protection Agency classifies 2,4-dinitrophenol, a phenol derivative, as a major pollutant. The manufacturing of polycarbonate resin, plastic, fragrances, textiles, and petroleum refineries are only a few of the sectors that employ all phenolic compounds extensively [2,3]. Numerous techniques are used to detoxify phenolic compounds, which are contaminants in polluted water, due to their ubiquitous production and the health and environmental dangers associated with them. Due to its advantages, such as cheap cost and environmental friendliness, biopolymers employed for detoxification have emerged as a viable and practical method to deal with numerous refractory contaminants, such as 2,4-dinitrophenol. Numerous studies have been done on the removal of phenolic compounds using fungus and bacteria [4], but very little has been done on utilizing algae [2]. The biodegradation of phenol by microalgae occurs only under aerobic conditions. The phenol metabolism ability of algae coupled with the potential applicability of the spent biomass as a biofuel feedstock and animal feed makes it a potential candidate for an environmentally sustainable process.

Materials and Methods

Preparation of CMC/Ag2O and CMC/Fe2O3 nanocomposites In this method, an aqueous solution of metal salt (0.1M) was prepared, and a CMC (2 g) was added to 100 mL of this solution. The system was kept under stirring (500 rpm) at room temperature for 30 min. Thereafter, 0.5M of sodium borohydride was added to the solution containing the metal ions loaded CMC under continuous stirring for 1 h. prepared metal oxide loaded CMC was isolated, washed with distilled water, and dried in an oven at 60oC for 24 h, and labelled as CMC/Ag and CMC/Fe.

Preparation of CMC/Ag2O-Fe2O3 nano-hybrid Freshly prepared aqueous solution from silver nitrate (0.1M) was added to the labelled samples as CMC/Fe with continuous stirring thereafter, 0.5M of sodium borohydride was added. The obtained silver-loaded CMC/Fe was labelled as CMC/Ag-Fe.

Coating method Prepared nanohybrid materials was applied to glassy carbon electrode (GCE) as following, 10 mg of material was mixed with 1.5 ml of isopropanol in a small container. Then, the tightly closed container was placed into a sonication bath for 10 min. After that, a drop of 5% Nafion solution was added, and the container was placed again into the sonication bath for an additional 5 min. The suspension became ready to be cast on the surface of GCE. A drop of the suspension was cast on the surface of GCE and then left to dry at room temperature.

Results DISCUSSION

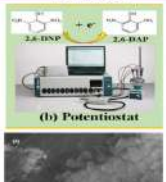

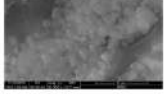

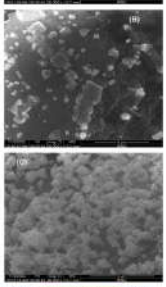

Figure 2: Scanning electron images of (a) CMC/Ag; (b) CMC/Fe and CMC/Ag-Fe

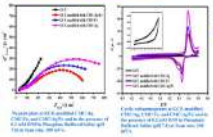

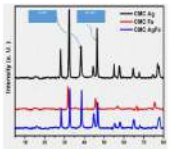

X-ray diffraction patterns for CMC/Ag, CMC Fe & CMC Ag/

In this work, CMC/Ag, CMC/Fe, and CMC/Ag/Fe-modified glassy carbon electrode (GCE) was prepared and used to examine the electrochemical oxidation behavior of 2,4-dinitrophenol (DNP) by cyclic voltammetry as presented in Figure 3. When compared to the getative GCE, the oxidation peak current of DNP at the modified GCE electrode was clearly higher. Demonstrating that the CMC/Ag, CMC/Fe, and CMC/Ag-Fe exhibit an exceptional enhancing impact on the electrochemical oxidation of DNP. Based on this, a quick and accurate electrochemical approach for the measurement of DNP was examined. The composite structure's impact was investigated. The center of the DNP's oxidation peaks in CMC/Ag + CMC/Fe > CMC/Ag/Fe. In the first step, the oxidation of DNP results in the formation of phenol and quinonic chemicals as well as the release of the nitro groups from the aromatic ring. These organics are converted into carboxylic acids in the subsequent phase (maleic, malonic and oxalic acid). Carbon dioxide is the product of the end procedure. The proposed information was also used to remove DNP from water samples. Additionally, the sensitivities of the electrodes is very simple, and the modified material was inexpensive and simple to gain. Figure 3 displays the results of N-purge plots at GCE-modified CMC/Ag, CMC/Fe, and CMC/Ag/Fe and in the presence of 0.2 mM DNP in Phosphate Buffered Saline (pH: 7.0) at Scan rate: 100 mV/s. A sensitivity was clearly visible for the modified GCE with CMC/Ag, CMC/Fe, and CMC/Ag/Fe nanocomposites to DNP, demonstrating the existence of a new charge-transfer method of DNP electrooxidation. When the electrode material is changed from CMC/Ag, CMC/Fe, and to CMC/Ag/Fe, the polarization resistance decreases, which indicates improved electrolyte-electrode interaction in the case of the CMC/Ag/Fe electrode when compared to the CMC/Ag, CMC/Fe electrodes and supports improved electron transfer for the CMC/Ag/Fe electrode.

Conclusion

In conclusion this project is to produce an ecofriendly, easy effective nanomaterials for wastewater treatment. A new promises Ag, Fe, and Ag nanoparticles-doped-Fe nanoparticles were encased in carboxymethyl cellulose (CMC/Ag, CMC/Fe, and CMC/Ag-Fe). The optical, structural, morphological, properties of prepared nanohybrid materials were thoroughly characterized using FESEM, XRD. Using a glassy carbon electrode (GCE) embellished with a wet-chemically produced CMC/Ag-Fe electro-catalyst, cyclic voltammetry (CV) and electrochemical impedance spectroscopy (EIS) methods were used to investigate the electrochemical oxidation-reduction of 2,4-dinitrophenol (2,6-DNP). The developed catalyst therefore offers a potential method for the effective oxidation and reduction of contaminants from industrial effluents.

References

1. Nasr M, Rafiq A, Ikram M, Haider A, Ahmad SOA, Haider J & Naz S. Elimination of dyes by catalytic reduction in the absence of light: A review. J Water Sci. 36 (2021) 15572. 2-16. Peng F, He Y, Zhou C, Su S & Lei B. The carbon nanotube-based materials and their applications for organic pollutant removal: A critical review. Chin Chem Lett. 32 (2021) 1426

Future Scholars Program 2023

برنامج علماء المستقبل 2023

Artificial intelligent aided in medicine

Professor.Ossama Zakarya
Ali Alkhars-Ahmed Alahmed-Fahad Almulhim-
Ammar AlOmair-Abdullah Bushid

Integration of Artificial intelligence (AI) to a primitive robot module to the management disaster conditions

Abstract

Natural disasters such as volcanos, earthquakes and buildings fallings pose a great challenge for medical and paramedical teams. They usually result in devastating outcomes. They may also lead to severe morbidities or even mortalities. Triage is a known protocol to deal with multiple injuries during disasters. The main challenging issue in triage is the medical team shortage. Therefore, we are proposing the current preliminary model of an AI aided robot to solve this problem.

Introduction

Many trials were advocated to make the triage system more successful despite of manpower shortages. Recently, it has been successfully preformed during the Russian-Ukrainian war with highly promising outcomes. Artificial intelligence (AI) is the main pivot for this mechanism. This is based on the notion that AI was successfully and effectively used in many aspects of life such as car production, medical instruments for diagnosis and/or even treatment of some tumors. It also proved to have a paramount role during the Covid-19 global pandemic saving the life of the medical team and controlling the propagation of the disease. The current work aimed to gauge the effectiveness of an Ai aided primitive robotic module in dealing with medical and surgical situations during disasters

Materials and Methods

An experimental triage took place evolving a preliminary module that is based on sharing photos taken via a robotic camera in relation to an AI loaded bank of similar images. Correlations between the taken photos and the AI stored data would take place aiming to evaluate the sensitivity and validity of the obtained results

Results

Based on a bunch of photos that were fed to the AI program, wounds were categorized into different subtypes. These include; burn wounds, cut wounds, surgical wounds, and deep and superficial ulcers. The module would take photos for different similar categories. The reliability and validity of the program proved to be higher than 95% within the five studied categories.

Discussions

Robots are currently gaining popularity in the medical and surgical fields.-(Barakat-johnson et al.,2022) Clinicians and patients are mostly admiring the newly advocated AI programs in medical and surgical diagnosis and treatment. Nevertheless, it is a high-priority hot topic in the management of battle and disaster fields with highly encouraging results

Conclusion

The proposed AI primitive robot module proved to be valid in the management of medical and surgical disasters. Further studies are needed to verify the accuracy of the technique to be widely adopted on a commercial basis.

References

(1)Barakat-Johnson, M., Jones, A., Burger, M., Leong, T., Frost-Gill, S., Barnett, A., ... & Lyons, F. (2022). Reshaping wound care: Evaluation of an artificial intelligence app to improve wound assessment and management amid the COVID-19 pandemic. International Wound Journal, 19(6), 1363-1372.

(2) Freedom's medical robot to treat injured soldiers.

Future Scholars Program 2023

برنامج علماء المستقبل 2023

Antibacterial activity of clove (*Syzygium aromaticum*) essential oil against foodborne pathogens

Zainab Rafee Abdullah Alelaiwi
Dr. Sallah A. A. Al-Hashedi and Prof. Dr. Khaled Ramadan

Paper
Engineering and Manufacturing Track

Abstract

Background and Aim: Clove (*Syzygium aromaticum* L. Myrtaceae) is an aromatic plant widely cultivated in tropical and subtropical countries, rich in volatile compounds and antioxidants such as eugenol, β-caryophyllene, and α-humulene. Compared with sodium benzoate, potassium sorbate and other chemical food preservatives, clove oil, the main volatile constituent of *S. aromaticum*, expresses various advantages on antimicrobial activity, aromas, and safety, and is an ideal substitute of chemical food preservatives. clove essential oil has received considerable interest due to its wide application in the perfume, cosmetic, health, medical, flavouring, and food industries. clove essential oil has biological activity relevant to human health, including antimicrobial, antioxidant, and insecticidal activity (Haro-González et al. 2021).

Methods: clove essential oil has biological activity CEO sunflower oil lotion effect broad-1 at tested organisms (Gram positive and negative strains) pathogenic bacteria ; foodborne diseases and tests inhibitory effects toward all lactic acid bacteria in probiotic bacteria such as *Lactobacillus* lactic subsp. lactis.

Conclusion: It was concluded that clove essential oils have emerged as effective antibacterial agents by showing high antibacterial activity against Pseudomonas aeruginosa, *E. coli*, and Staphylococcus aureus, as evidenced by the inhibition zone diameter in well assay method. So, we can recommend it as food preservation material.

Keywords: clove (*Syzygium aromaticum*), essential oils, *Escherichia coli*, Lab. deBrosa40 subsp. *bulgaricus*, well assay.

Introduction

The information of foodborne illnesses and outbreaks caused by foodproducing animals is important in human health and food industry. Contaminated food results in 600 million cases of foodborne diseases are 420,000 deaths worldwide every year (Lee and Yoon, 2021).

Clove (*Syzygium aromaticum* L., Myrtaceae) is an aromatic plant widely cultivated in tropical and subtropical countries, rich in volatile compounds and antioxidants such as eugenol, β-caryophyllene, and α-humulene (Haro-González et al. 2021). Use of spices as colorants and preservatives is booming function in the food industry, and among these spices, clove (*Syzygium aromaticum*) is of great importance (Jirovetz et al., 2017). Compared with sodium benzoate, potassium sorbate and other chemical food preservatives, clove oil, the main volatile constituent of *S. aromaticum*, expresses various advantages on antimicrobial activity, aromas, and safety, and is an ideal substitute of chemical food preservatives.

Eugenol, the most important component of clove oil, has been accepted as food preservatives by China, the United States, the European Union, and other countries and regions. Clove essential oil has received considerable interest due to its wide application in the perfume, cosmetic, health, medical, flavouring, and food industries. clove essential oil has biological activity relevant to human health, including antimicrobial, antioxidant, and insecticidal activity (Haro-González et al. 2021).

Many oral care product products containing clove oil have appeared on the market in China, these products express beneficial effects on halitosis, dental plaque, oral tiredness, and allergic pain of tooth (Ho et al. 2018). Several reports suggest that *S. aromaticum* L. contains approximately 70-90% wt. of clove bud essential oils (CEO) contains a high amount of phenolic compounds with several biological activities, including antibacterial, antifungal, insecticidal, and antioxidant properties (Tunc and Kloss, 2016). The FDA classifies CEO as generally recognized as safe (GRAS) for this reason, it is used in perfumes, cosmetics, sanitary products, medicines, and foods (Hacı-Dönmez et al. 2021).

Materials and Methods

1. Bacteria and growth media

Bacterial strains (ATCC and DSM stocks) used as indicators for clove essential oil evaluation for antimicrobial activities are shown in Table (1). Lactic acid bacteria (LAB), reference strains, were propagated in MRS broths (Oxoid, UK) at 37°C in 1% (v/v) of 48 h and pathogenic bacteria (indicators) were activated in Brain Heart Infusion (BHI) broth (Oxoid, UK) at 24°C. is 1° for 24h ±2. Working culture (LAB and other indicators) were maintained at 4°C in MRS+1.5% agar (deep agar for LAB) or slants of BHI +1.5% agar for (indicators). LAB stock cultures were maintained at -20°C in MRS broth containing sterile 10% (v/v) glycerol and pathogens were kept at -20°C in BHI (10% sterile glycerol). Prior to use each strain was activated twice in the appropriate broth and conditions. Stab or slant cultures were transferred and activated bimonthly for making new working cultures.

2. Disc Assay Method

Susceptibility of the 5 reference strains isolates (Table 3) to 5 type of antibiotics was performed by the disc diffusion method (Kirby-Bauer technique, as recommended by National Committee for Clinical Laboratory Standards (NCCLS) and as described by Kissi (2000). Commercially available antibiotics disc (Oxoid, UK) Vancomycin (5 µg) Wk), Kanamycin (30 µg) K30, Amoxycillin (30 µg) AMC30, Tetracycline (30 µg) T030, and Chloramphenicol (30 µg) C30, were placed on the surface of the agar plates.

Liquid cultures of the 5 reference strains were incubated overnight at 37° C, and then were diluted by sterile peptone (0.1% v/v) to reach a count of 10⁶ CFU/ml. Sterilized 150 ml Nutrient Agar (Oxoid, UK) were tempered to 48°C (water bath) prior to seeding with 100µl (10⁶ CFU/ml) of diluted culture from the indicators listed in Table (3). Plates were incubated (24h) at 37° C (5 discs per plate, each in replicate plate). After incubation, the diameter of the zones of inhibition was measured.

3. Activity Spectrum of Clove essential oil (CEO)

Antimicrobial activity for CEO were screened using disc agar well diffusion test (well assay) of Nowaka et al., 2006). Sterilized 150 ml Nutrient Agar (Oxoid, UK) were tempered to 48°C (water bath) prior to seeding with 100µl (10⁶ CFU/ml) of diluted cultures from the indicators listed in Table (3). Inoculated media were poured into Petri plates (in replicates) then left to harden under room temperatures. Wells (6 mm in diameter) were made in the agar with a sterile Cork borer (stainless steel borer) and each well was filled with 100µl of CEO. Plates were left at room temperatures for 30 min to allow diffusion of CEO. Inhibition zones (including well diameter) around wells were measured in mm after incubation at 37° C. Clear zones greater than 8 mm were considered as active CEO against the indicator. Zones of inhibition were measured and the average zone size of each dilution was taken.

Table (1). Indicator bacteria used in the study

Bacteria	Source
Lactic Acid Bacteria (LAB)	
Lact. acidophilus subsp. bulgaricus	DSM10892
Lactococcus lactis subsp. lactis	DSM20481
Streptococcus thermophilus	DSM20617
Pathogenic and Spoilage Bacteria	
Escherichia coli (Migula)	ATCC 25922
Staphylococcus aureus	ATCC 25923
Pseudomonas aeruginosa	ATCC 27853
Aeromonas hydrophila	ATCC 35654
Acinetobacter calcoaceticus	ATCC 19002
Proteus mirabilis	ATCC 29906
Salmonella typhimurium	ATCC 14028

Table (2). Sensitivity of Reference bacteria to Clove essential oil (CEO) using the well assay, inhibition zone (mm).

CEO	Pathogenic Bacteria (Antibiotic discs)/mm				Lactic acid bacteria (LAB)	
	Gram negative bacteria		Gram positive bacteria			
	SE76	PA53	EC32	S505	SA12	LM44	LB81	LL55	ST17
100 µL/L	14	20	11	15	22	18	14	19	15
50 µL/L	12	15	10	12	19	14	12	—	12
25 µL/L	—	12	11	12	15	12	—	—	—
12 µL/L	—	11	—	9	12	—	—	—	—

* Refer to Table (1) "—" no inhibitions.

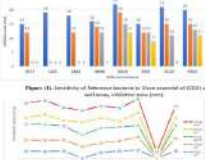

Figure (1). Sensitivity of Reference bacteria to Clove essential oil (CEO) using the well assay, inhibition zone (mm).

Figure (2). Inhibition zones tested for antibiotic disc against tested bacteria.

Picture (1). Zones of inhibition caused by different antibiotic discs against staphylococcus aureus (ATCC 25923) using disc diffusion assay.

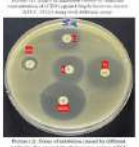

Picture (2). Zones of inhibition caused by different antibiotic discs against staphylococcus aureus (ATCC 25923) using disc diffusion assay.

Discussions

Clove essential oils were active in inhibiting *E. coli* ATCC 25922, *K. pneumoniae* ATCC 700603), the antibacterial activity of cloves has been widely reported (Hoque et al., 2008; Dhara and Tripathi, 2010). In this study, we tested the antibacterial activity of clove essential oils against standard pathogens bacteria and lactic acid bacteria as a comparison to the previous studies.

Eugenol showed strong antibacterial activity against both pathogenic and probiotic microorganisms as (*Lactococcus lactis* subsp. *cremoris*, *Lactobacillus delbrueckii* subsp. *bulgaricus*, *Lactobacillus casei*, *Lactobacillus rhamnosus*, and *Lactobacillus paracasei* subsp. *paracasei* (Gutt emer. et al., 2007). However, in the colon of mice (*in vivo*), eugenol treatment leads to an increase in abundance of specific families within the Clostridiales order, and confers colonization resistance to the enteric pathogen such as *Citrobacter rodentium*, which is benefit to strengthen the mucosal barrier and protect against invading pathogens and disease (Wlodarska, et al., 2015). It should be noted that the cytotoxicity of clove oil and eugenol is obtained from *in vitro* or *in vivo* study, and there is no report on the damage of them on human body, which should be given further research.

Conclusion

This study reveals that clove essential oils have emerged as effective antibacterial agents by showing high antibacterial activity against each bacterium tested. Indicated by the inhibition zone diameter in well assay value. On the basis of the data, clove essential oils can be recommended as bioactive compounds to control the spread of pathogens bacteria.

In summary, clove oil and its main component eugenol express inhibition on Gram-negative bacteria as *E. coli*, *Salmonella*, and *P. aeruginosa*, and Gram-positive bacteria as *Staphylococcus*, and *L. monocytogenes*. Based on these antimicrobial activities, clove oil has a good research and application value in the food preservation field.

References

Ahmad I, Jamil Beyatli Y (2003). Antibacterial activity of Juniperus communis L. and Juniperus oxycedrus L. essential oils. Journal of Environmental Biology 24: 243-248.

Ali A, Chen C, Mahomoodally MF, Pittchar JN, Sultana K, Ahmed S (2019). Potential of essential oils for therapeutic and industrial applications. In: Essential oils-oils of nature. IntechOpen. https://doi.org/10.5772/intechopen.88413

Bakkali F, Averbeck S, Averbeck D, Idaomar M (2008). Biological effects of essential oils–a review. Food and chemical toxicology 46: 446-475. https://doi.org/10.1016/j.fct.2007.09.106

Bassolé IHN, Juliani HR (2012). Essential oils in combination and their antimicrobial properties. Molecules 17: 3989-4006. https://doi.org/10.3390/molecules17043989

Bhavaniramya S, Vishnupriya S, Al-Aboody MS, Vijayakumar R, Baskaran D (2019). Role of essential oils in food preservation: recent developments. Enzyme and microbial technology 130: 109395. https://doi.org/10.1016/j.enzmictec.2019.109395

Burt S (2004). Essential oils: their antibacterial properties and potential applications in foods—a review. International journal of food microbiology 94: 223-253. https://doi.org/10.1016/j.ijfoodmicro.2004.03.022

Dhara L, Tripathi A (2010). Antibacterial activity of *Eucalyptus citriodora* essential oil and synergy with gentamicin. Indian Journal of Pharmaceutical Sciences 72: 669. https://doi.org/10.4103/0250-474X.78525

Gutt emer. et al., 2007. Investigation of bacteriocin-like activity of a novel strain of lactic acid bacteria isolated from Kefir. Lett Appl Microbiol 44: 213-218.

Hoque MM, Bari ML, Inatsu Y, Juneja VK, Kawamoto S (2008). Antibacterial activity of cloves and cinnamon bark extracts against foodborne pathogens in relation to storage temperature. Food Control 19: 811-818. https://doi.org/10.1016/j.foodcont.2007.08.008

Jirovetz L, Buchbauer G, Stoyanova AS, Georgiev EV, Damianova ST (2006). Composition, quality control and antimicrobial activity of the essential oil of long-time stored flowers of Rosa damascena Mill. from Bulgaria. Journal of Essential Oil Research 18: 359-362. https://doi.org/10.1080/10412905.2006.9699113

Kissi M (2000). Antibacterial activity of Moroccan spices. Journal of Essential Oil Research 12: 249-254. https://doi.org/10.1080/10412905.2000.9699504

Lee J, Yoon Y (2021). Modeling the Growth of Pathogens in Food Products: Review of the Development of Predictive Models and Their Limitations. Microorganisms 9: 1-19. https://doi.org/10.3390/microorganisms9010119

Nowaka A, Buchwald A, Krasniewska K, Kahlina K, Gniewosz M (2006). Antimicrobial activity of plant essential oils against *Escherichia coli* O157:H7 and *Staphylococcus aureus* on model meat stored in different conditions. International Journal of Food Science & Technology 41: 1-6. https://doi.org/10.1111/j.1365-2621.2006.01178.x

Ogata-Arakaki D, Motooka D, Yamamoto N, Furuta M, Nakamura S, Iida T, Izumi H (2020). Novel Lactobacillus species and strains, and the relationship between the abundance of Lactobacillus species and histamine concentration in Japanese soy sauce moromi. International Journal of Food Microbiology 331: 108753. https://doi.org/10.1016/j.ijfoodmicro.2020.108753

Pandey AK, Kumar P, Singh P, Tripathi NN, Bajpai VK (2017). Essential oils: sources of antimicrobials and food preservatives. Frontiers in microbiology 7: 2161. https://doi.org/10.3389/fmicb.2016.02161

Tunc I, Kloss F (2016). Antimicrobial activity of selected plant essential oils and some of their components. Journal of Essential Oil Research 28: 1-8. https://doi.org/10.1080/10412905.2015.1090000

Wlodarska M, Kamada N, Bhinder G, Raffatellu M, Kelly CR, Bäumler AJ, Finlay BB (2011). Antibiotic treatment alters the colonic mucus layer and predisposes the host to exacerbated *Citrobacter rodentium*-induced colitis. Infection and immunity 79: 1536-1545. https://doi.org/10.1128/IAI.01104-10

Determination of Mass attenuation coefficients for Gamma-rays in building materials-Application for Saudian building materials

Mohammed Ahmed Albassan
Supervision : Dr. Fouad Gharbi

College of Science/Department of Physics

Abstract

A Geant4 Monte Carlo code was developed for the calculation of Gamma-ray mass attenuation coefficients for building materials for energy less than 2 MeV and validated from theoretical computations in Xcom. The code was validated by comparison with experimental and theoretical values of attenuation coefficients from XCOM database, as well as with comparisons with other Monte Carlo published calculations such as those using MCNP code for pure and mixtures of building materials. The developed code in this work is a good alternative to experimentation. An application this code has been used to calculate the mass attenuation coefficients of the Spectroscopy for Saudian cement.

Results

The developed Geant4 code has been used for mass attenuation coefficients calculation for Cement, Gypsum, and Admixture of Gypsum, PE/CEO and Cement, PE/CEO, and pure building materials Concrete (Concrete and Cement@ 0). The calculated mass attenuation coefficient for samples Gypsum with PE/CEO and other building materials for the four energies of 356.0, 661.6, 1,173.2 and 1,332.5 keV are shown in Figure 3 to 5. Figure 2 compares the mass attenuation coefficients of Cement, Gypsum, the mixtures (Cement and PE/CEO) (Gypsum and PE/CEO), and concrete (Concrete and Cement@ 0) with the theoretical values from XCOM for energy of 662 keV. The results from mass attenuation coefficients of pure and doped cement or cement are interesting with the increase of photon energy. The variation of mass attenuation coefficient can be explained using the fundamental photon interaction process of the photoelectric effect, Compton effect, and pair production for low, intermediate, and high energy photons, respectively, which agrees with atomic number of the chemical elements composing the material. There is a noticeable difference in the mass attenuation coefficients of PE/CEO doped Cement, and Gypsum between low energy (photoelectric effect zone) and high energy (pair formation region). Because PE/CEO has atomic densities intermediate to the photoelectric effect zone (photoelectric cross section $\sigma_{pe} \propto Z^4/E^3$) and pair production zone ($\sigma_{pp} \propto Z^2$), the mass attenuation coefficients are higher compared with experimental and theoretical results. As $E \to \infty$, the mass attenuation coefficients of Cement and any XCOM results for the samples, in addition, MCNP and other experimental results are known to be non-transparent than the Geant4 simulation results.

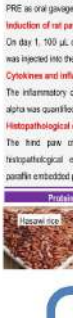

Discussions

The calculation of mass attenuation coefficients for cement using the Monte Carlo Geant4 code without simulation is found to be better and more accurate than using the Geant4 with interaction in an in Tables 1 and 2 as the XCOM is a review and very close to the XCOM results as shown in Figure 1.

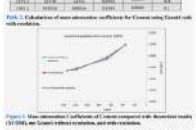

Unit 1 : Calculation of mass attenuation coefficients for Cement using Geant4 code without simulation.

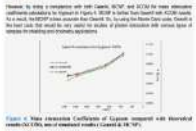

Unit 2: Calculations of mass attenuation coefficients for Cement using Geant4 code with simulation.

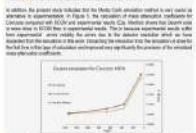

Figure 1: Mass attenuation Coefficients of Cement compared with theoretical results (XCOM), our Geant4 without simulation, and with simulation.

However, by using a comparison with both Geant4, XCOM and XCOM for mass attenuation coefficients calculation in Figure 2, XCOM is better than Geant4 with XCOM results. As a result, the MCNP is more accurate than Geant4. So, by using the Monte Carlo code, Geant4 is the best code that should be very useful for studies of photon interaction with various types of samples for shielding and dosimetry applications.

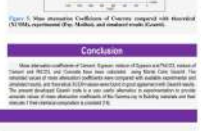

Figure 2: Mass attenuation Coefficients of Cement compared with theoretical results (XCOM), our Geant4 without simulation, and with simulation.

In addition, the present study indicates that the Monte Carlo simulation method is very useful as alternative to experimentation. In Figure 3, the calculation of mass attenuation coefficients for Concrete compared with XCOM and experimental results (Cp). Monte Carlo Geant4 code is more close to XCOM than in experimental results. This is because experimental results suffer from experimental errors mainly the errors due to the detector resolution which we have discarded from the simulation in this work. Discarding the simulation from the resolution of detector the final line in the type of calculation and improved very significantly the precision of the simulated mass attenuation coefficients.

Figure 3: Mass attenuation Coefficients of Concrete compared with theoretical (XCOM), experimental (Exp. Medium), and simulated results (Geant4).

Conclusion

Mass attenuation coefficients of Cement, Gypsum, mixtures of Gypsum and PE/CEO, mixtures of Cement and PE/CEO, and Concrete have been calculated using Monte Carlo Geant4. The calculated values of mass attenuation coefficients were compared with available experimental and theoretical values from XCOM database and other published calculations using MCNP code. The present developed Geant4 code is a very useful alternative to experimentation to provide accurate values of mass attenuation coefficients of the Gamma-ray in building materials and their mixtures if their chemical composition is provided [19].

References

[1] Hubbell, J. H. (1982). Photon mass attenuation and energy-absorption coefficients. The International Journal of Applied Radiation and Isotopes, 33(11), 1269-1290.

[2] Hubbell, J. H., & Seltzer, S. M. (1995). Tables of X-ray mass attenuation coefficients and mass energy-absorption coefficients 1 keV to 20 MeV for elements Z= 1 to 92 and 48 additional substances of dosimetric interest (No. PB-95-220539/XAB; NISTIR-5632). National Inst. of Standards and Technology-PL, Gaithersburg, MD (United States). Ionizing Radiation Div.

[3] Berger, M. J., Hubbell, J. H., Seltzer, S. M., Chang, J., Coursey, J. S., Sukumar, R., ... & Olsen, K. J. (2010). XCOM: photon cross sections database (version 1.5). National Institute of Standards and Technology, Gaithersburg, MD.

[4] Seltzer, S. M., & Hubbell, J. H. (1995). Tables and graphs of photon-interaction cross sections from 10 eV to 100 GeV derived from the LLNL evaluated photon data library (EPDL). Radiation Research Society.

[5] Hubbell, J. H., & Seltzer, S. M. (1996). Tables of X-ray mass attenuation coefficients and mass energy-absorption coefficients 1 keV to 20 MeV for elements Z= 1 to 92 and 48 additional substances of dosimetric interest (No. PB-95-220539/XAB; NISTIR-5632). National Inst. of Standards and Technology-PL, Gaithersburg, MD (United States). Ionizing Radiation Div.

[6] Berger, M. J., Hubbell, J. H., Seltzer, S. M., Chang, J., Coursey, J. S., Sukumar, R., ... & Olsen, K. J. (2010). XCOM: photon cross sections database (version 1.5). National Institute of Standards and Technology, Gaithersburg, MD.

[7] Seltzer, S. M., & Hubbell, J. H. (1995). Tables and graphs of photon-interaction cross sections from 10 eV to 100 GeV derived from the LLNL evaluated photon data library (EPDL). Radiation Research Society.

[8] Hubbell, J. H., & Seltzer, S. M. (1996). Tables of X-ray mass attenuation coefficients and mass energy-absorption coefficients 1 keV to 20 MeV for elements Z= 1 to 92 and 48 additional substances of dosimetric interest (No. PB-95-220539/XAB; NISTIR-5632). National Inst. of Standards and Technology-PL, Gaithersburg, MD (United States). Ionizing Radiation Div.

[9] Berger, M. J., Hubbell, J. H., Seltzer, S. M., Chang, J., Coursey, J. S., Sukumar, R., ... & Olsen, K. J. (2010). XCOM: photon cross sections database (version 1.5). National Institute of Standards and Technology, Gaithersburg, MD.

[10] Seltzer, S. M., & Hubbell, J. H. (1995). Tables and graphs of photon-interaction cross sections from 10 eV to 100 GeV derived from the LLNL evaluated photon data library (EPDL). Radiation Research Society.

[11] Hubbell, J. H., & Seltzer, S. M. (1996). Tables of X-ray mass attenuation coefficients and mass energy-absorption coefficients 1 keV to 20 MeV for elements Z= 1 to 92 and 48 additional substances of dosimetric interest (No. PB-95-220539/XAB; NISTIR-5632). National Inst. of Standards and Technology-PL, Gaithersburg, MD (United States). Ionizing Radiation Div.

[12] Berger, M. J., Hubbell, J. H., Seltzer, S. M., Chang, J., Coursey, J. S., Sukumar, R., ... & Olsen, K. J. (2010). XCOM: photon cross sections database (version 1.5). National Institute of Standards and Technology, Gaithersburg, MD.

[13] Seltzer, S. M., & Hubbell, J. H. (1995). Tables and graphs of photon-interaction cross sections from 10 eV to 100 GeV derived from the LLNL evaluated photon data library (EPDL). Radiation Research Society.

[14] Hubbell, J. H., & Seltzer, S. M. (1996). Tables of X-ray mass attenuation coefficients and mass energy-absorption coefficients 1 keV to 20 MeV for elements Z= 1 to 92 and 48 additional substances of dosimetric interest (No. PB-95-220539/XAB; NISTIR-5632). National Inst. of Standards and Technology-PL, Gaithersburg, MD (United States). Ionizing Radiation Div.

[15] Berger, M. J., Hubbell, J. H., Seltzer, S. M., Chang, J., Coursey, J. S., Sukumar, R., ... & Olsen, K. J. (2010). XCOM: photon cross sections database (version 1.5). National Institute of Standards and Technology, Gaithersburg, MD.

[16] Seltzer, S. M., & Hubbell, J. H. (1995). Tables and graphs of photon-interaction cross sections from 10 eV to 100 GeV derived from the LLNL evaluated photon data library (EPDL). Radiation Research Society.

[17] Hubbell, J. H., & Seltzer, S. M. (1996). Tables of X-ray mass attenuation coefficients and mass energy-absorption coefficients 1 keV to 20 MeV for elements Z= 1 to 92 and 48 additional substances of dosimetric interest (No. PB-95-220539/XAB; NISTIR-5632). National Inst. of Standards and Technology-PL, Gaithersburg, MD (United States). Ionizing Radiation Div.

[18] Berger, M. J., Hubbell, J. H., Seltzer, S. M., Chang, J., Coursey, J. S., Sukumar, R., ... & Olsen, K. J. (2010). XCOM: photon cross sections database (version 1.5). National Institute of Standards and Technology, Gaithersburg, MD.

[19] Seltzer, S. M., & Hubbell, J. H. (1995). Tables and graphs of photon-interaction cross sections from 10 eV to 100 GeV derived from the LLNL evaluated photon data library (EPDL). Radiation Research Society.

Natural radioactivity in Saudian Building Materials

Waad Al-Ali
Supervision : F. Gharbi

College of Science/Department of Physics

Abstract

Natural radioactivity ^{232}Th, ^{226}Ra and ^{40}K in Saudian Building Materials used in Al-Ahsa region was measured using NaI gamma spectrometry based on 12 samples collected from the local markets at Al Ahsa region.

Average activity concentration was found equal to 33.10, 26.44 and 302.73 Bq/kg for ^{232}Th, ^{226}Ra and ^{40}K, respectively. Radioactive hazard indices relative to the studied building materials were evaluated. Notably, the Radium equivalent, the external hazard, the internal hazard indices and the indoor air absorbed dose rate, as well as the annual effective dose rate were determined. The obtained values of the radiological indices were less than their corresponding maximum international recommended limits. Which proves that the studied Saudian Building materials are safe for use.

Introduction

Humans are continuously exposed to ionizing radiation resulting from naturally and artificial sources of radioactivity [1]. The main source of natural radioactivity in buildings is the underlying soil and the building materials which constitutes the material of the walls, the floor and the ceiling. In this work we are interested to characterize radiologically the natural radioactivity due to Building Materials used in construction of the Saudian dwellings. The inhabitation is that spend most of their time (more than 8 hours a day) at home which could expose them to high level of natural radiation coming Building Materials. The radiological characterization is based on the measurement of the activity concentration of the three radionuclides ^{40}K, ^{226}Ra and ^{232}Th using Gamma spectrometry. Their determination allows to assess the radiation exposures through well defined radiological indices. These indices are the Radium equivalent activity, external hazard index, internal hazard index, indoor air absorbed dose rate and the gamma index [2]. In this work we used NaI gamma spectrometry to measure the concentration of these radionuclides in a collection of 12 Building Material samples collected from the local markets at Al-Ahsa region. It was ensured that all the collected samples were locally produced and not imported.

Materials and methods

12 samples (Figure 1) of building materials were collected from the local market of Al_Ahsa region. We ensured that the building materials were locally produced by factories from Saudi Arabia. The samples were homogenized of cement, sand and Gypsum samples were oven dried at a temperature of 105°C for 12 h, sieved through a 200 mesh and conditioned in polyethylene geometries of 100 cm³ volume. Each sample was left 4 weeks before exposition to allow for the secular equilibrium between ^{226}Ra and ^{232}Th and their progenitors. Measurement of radioactivity was performed with a 3x3 inch NaI scintillation detector employing a lead shielding to reduce the perturbation of the measurement process by the Background radiation. In order to reduce more the effect of the background radiation an empty geometry acquisition was performed for a duration of 130000 s and the obtained spectrum was subtracted from the spectra relative to the samples. **GammaVision** Ortec Software was used to calibrate the detector (Figure 2 and 3) and to measure the count rate relative to each emission energy of interest in the obtained spectra. ^{226}Ra radionuclide was estimated from the 351.9 keV (35.7% γ peak of ^{214}Pb and 609.3 keV (46.1%), 1120.3 keV (15%), 1238.6 keV (5.83%) and 1764 keV (15.9% γ peaks of ^{214}Bi. ^{232}Th radionuclide was estimated from the 911.2 keV (25% γ-ray of ^{228}Ac, 238.6 keV (43.6% γ-peak of ^{212}Pb and 583.1 kev (84.5 γ-peak of ^{208}Tl. ^{40}K radionuclide was estimated using 1,461 keV (10.7% γ- peak from ^{40}K itself.

The activity concentration A (Aq/kg) is determined according to :

$$A\,(Bq/kg) = \frac{(N/T)}{\varepsilon \times P \times m}$$

Where :
N/T : is the count rate corrected by subtracting the count due to the Background radioactivity (s⁻¹).
ε : The full energy peak efficiency.
P : The emission probability.
m : Mass of the sample (kg)

Figure 1: Samples of Building Materials

We calculated the following radiological indices [2] for each sample of studied building material in this work (Table 1)

$$H_{ex} = (A_{Ra}/370) + (A_{Th}/259) + (A_K/4810)$$

$$Ra_{eq} = A_{Ra} + 1.43\,A_{Th} + 0.077\,A_K$$

$$H_{in} = (A_{Ra}/185) + (A_{Th}/259) + (A_K/4810)$$

$$I_\gamma = (A_{Ra}/300) + (A_{Th}/200) + (A_K/3000)$$

Results

Obtained activity concentrations and determined radiological indices for the studied samples of Building Materials are illustrated in Table 1.

Table 1. Obtained activity concentrations and calculated radiological indices relative to the studied Saudian Building Materials.

Samples	^{40}K (Bq/kg)	^{226}Ra (Bq/kg)	^{232}Th (Bq/kg)	Ra_{eq}	H_{ex}	H_{in}	I_γ
Cem01	183.61	32.15	11.87	59.80	0.20	0.26	0.17
Cem02	213.41	34.51	15.20	64.28	0.23	0.28	0.19
Cem03	290.71	46	19.97	85.72	0.30	0.40	0.26
Cem04	404.81	29.79	12.20	67.82	0.25	0.28	0.27
Sand01	324.07	33.28	27.17	101.51	0.34	0.39	0.36
Sand02	370.84	39.08	29.85	98.80	0.33	0.38	0.33
Sand03	270.40	42.29	24.24	78.06	0.28	0.40	0.29
Sand04	461.44	51.38	31.95	83.83	0.27	0.36	0.36
Sand05	0.00	12.2	13.47	111.28	0.38	0.56	0.31
Gypsum	0.00	11.10	20.31	92.74	0.30	0.39	0.29
Gyps02	0.00	19.01	17.80	82.06	0.31	0.38	0.28
Gyps03	0.00	18.04	20.87	73.46	0.29	0.40	0.41
Average	302.73	26.44	33.10	73.85	0.26	0.35	0.33

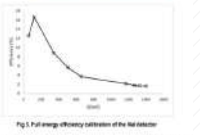

Fig 1. Full energy efficiency calibration of the NaI detector

Calibration of the detector was performed experimentally for point source configurations and an efficiency transfer procedure was then applied to transfer the experimental point source efficiency to the desired volumetric detector configuration. The transfer procedure was performed using Monte Carlo method. The experimental validation of the efficiency of the transfer method was realized for point sources.

Figure 3 illustrates the full energy calibration of the detector which is obtained by fitting the obtained values of the efficiency relative to the emission energy values with logarithmic function. Errors on the obtained activity due to the calibration procedure do not exceed 5 %. The errors due to the whole measurement procedure do not exceed 15 % for all the determined activity concentrations on this work.

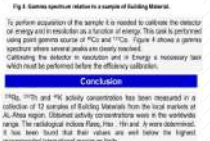

Fig 4. Gamma spectrum relative to a sample of Building Material.

To perform acquisition of the sample it is needed to calibrate the detector on energy and in resolution as a function of energy. This task is performed using point gamma source of ^{60}Co and ^{137}Cs. Figure 4 shows a gamma spectrum where several peaks are clearly resolved.

Calibrating the detector in resolution and in Energy a necessary task which must be performed before the efficiency calibration.

Discussion

The measured activity concentrations of Building Materials in this work were found to be in the range of the worldwide average values.

All the obtained **Ra_{eq}** values (see table 1) are significantly less than the recommended safe limit value 370 Bq/kg [3]. The mean value of **Ra_{eq}** obtained for the present building materials is 73.85 Bq/kg. It is very low compared to the safe limit recommended value.

Columns 6 and 7 in table 1 show that all the obtained **H_{ex}** and **H_{in}** indices values are both less than 1.

The gamma index I_γ is calculated as proposed by the European Commission [3]. Obtained I_γ values for the studied Building Materials do not exceed the maximum value 2 recommended European.

Experimentation

Fig 2. Gamma spectrometry and building materials samples

Conclusion

The activity concentrations of the samples have been measured in a collection of 12 samples of Building Materials from the local markets at Al-Ahsa region. Obtained activity concentrations were in the worldwide range. The radiological indices Ra_{eq}, H_{ex}, H_{in} and I_γ were determined. It has been found that their values are well below the highest recommended international maximum limits.

Saudian building materials in Al-Ahsa region according to the samples which have been studied are then found to be safe from the radiological point of view.

References

[1] N. Ibrahim, Journal of Environmental Radioactivity, vol. 45, no. 203 (1999).

[2] United Nations Scientific Committee on the Effects of Atomic Radiation, Sources and Risks of Ionizing Radiation. Report to the General Assembly, with scientific annexes, United Nations, (2008).

[3] I. Durrani and P. J. Statham, Health Phys., vol. 48, no. 87, (1985).

Immune modulatory effect of probiotic bacteria on inflammation in the mice model

Amjad Almajed and Aljawharah Alsubaie
Dr. Ashraf Khalifa and Dr. Hairul Islam Mohamed

Paper/ Patent
Track Biotechnology

Abstract

Three active probiotic bacterial isolates: ASF-1, ASF-2 and ASF-4 from the Al-Asfar lake, were screened for anti-inflammatory activity in in vivo mouse model. Edema was induced with 1% carrageenan. After 8 days, Paw of tested mouse were extracted and quantify the cytokines and histopathological examinations using H & E staining. The PRE treatment decreased by 32% and 28% in paw thickness. The histological inflammation were significantly reduced in PRE treated mice.

Introduction

The use of probiotic bacteria in dietary supplements is widely documented in the literature. *Lactobacillus* spp. have been used against many disease conditions. Probiotic characteristics microbes also known to express its **antimicrobial**, immunomodulatory and anti-arthritic properties. About 70–80% of the world's population demanding the nonconventional drugs strategies. In vivo approach of probiotic products will able to reduce the acute inflammation induced by carrageenan when tested in male mouse. In this study, protein from fermented Hasawi rice was evaluated against carrageenan induced paw edema in Balb/c mice and analyze the contribution to the upregulation of the powerful immunomodulatory agents.

Materials and Methods

Bacterial culture

Potential probiotics cultures were screened using in vitro characteristics tools. The active culture was used for Hasawi rice fermentation.

Preparation of prebiotics from probiotic fermented hasawi rice.

Protein rich extract (PRE) of potential probiotic fermented Hasawi rice were extracted and quantified the protein content using Bradford reagent assay. Antioxidant analysis was done using DPPH.

Assessment of the anti-inflammatory activity of probiotic strains on carrageenan-induced paw edema model in male Animals was done in compliance with code of ethics of King Faisal University

Experimental protocol

The experiment lasted for 8 days . The Balb/C mice were grouped as follows: (n = 6 per group): (i) Group A (saline control), (ii) Group B (carrageenan control), (iii) Group C (indomethacin group, a standard anti-inflammatory model), (iv) Group D received 1 mg of PRE as oral gavage fluid.

Induction of rat paw edema using carrageenan

On day 1, 100 µL of fresh (1%) carrageenan solution was injected into the right hind paw of each mouse.

Cytokines and inflammatory marker estimation

The inflammatory cytokines, IL-6, IL-1beta and TNF-alpha was quantified using Invitrogen Elisa mouse kit.

Histopathological of inflammatory changes

The hind paw of tested mouse was used for histopathological evaluation of the formalin fixed paraffin embedded paw tissue using the hematoxylin

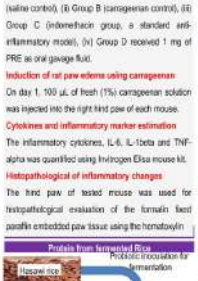
Protein from fermented Rice
Has

Chemical, surface, and thermal studies of mixed oxides cupric oxide (CuO), lanthanum oxide (La_2O_3), and graphene oxide for superior dye degradation from aqueous solution

Mohammed N. Almarri*
Dr. Hany M. Abd El-Lateef, Dr. M. Gouda,
College of Science/ Department of Chemistry
Journal of Materials Research and Technology (2023), IF= 6.267, Q1

Abstract

Mixed oxy- compositions are lately used for water treatment due might be exploited as photo-catalyst, and adsorptive materials for the disposal of water pollutants. Cupric oxide (CuO), lanthanum oxide (La_2O_3), and graphene oxide (GO)-based mixed oxides nanocomposites (NCs) show an interest in water treatment applications owing to the adsorptive feature of carbon-based nanoparticles (NPs), besides low band gap of metal oxides that boosts photo-catalytic process. CuO/La_2O_3/GO-based NCs are prepared and tested for their thermal stability, and dye removal activity. XRD, SEM, and TEM analyze the microstructural features of the different-mol compositions. Also, the bonding between GO, CuO, and La_2O_3 is approved with the FTIR spectrum. The change in NCs structure upon the incorporation of CuO and La_2O_3 into GO nanosheets is inspected via TEM micrographs showing a decline in lanthanes rod length to be 200 nm on average. Additionally, the improved roughness structure and the compact grain size appear in SEM micrographs report CuO grain size reduction reaching an average size of 290 nm. The roughness parameters of CuO/La_2O_3/GO are extraordinarily heightened in which the supreme value of roughness average is 74 nm. TNC exhibits a maximum value of 89% as a methylene blue (MB) dye removal agent. Thereafter, the fabricated NCs are recommended for water treatment due to their enriched physicochemical and morphological features as well as better thermal stability and exerted dye removal activity.

Results

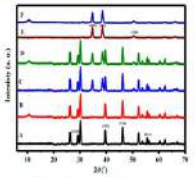

Figure 5: XRD of CuO, La_2O_3, and GO-based nanocomposites (A) La_2O_3, (B) La_2O_3/GO, (C) La_2O_3/CuO, (D) La_2O_3/CuO/GO, (E) CuO, and (F) CuO/GO.

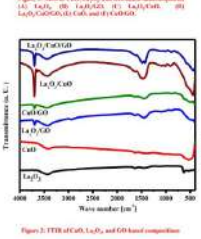

Figure 2: FTIR of CuO, La_2O_3, and GO-based composites

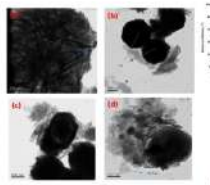

Figure 3: TEM micrographs of CuO, La_2O_3, and GO-based compositions where: (a) CuO, (b) La_2O_3/GO, (c) La_2O_3/CuO, and (d) La_2O_3/CuO/GO.

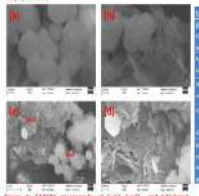

Figure 4: FESEM micrographs of CuO, La_2O_3, and GO-based compositions where: (a) CuO, (b) La_2O_3/GO, (c) La_2O_3/CuO, and (d) La_2O_3/CuO/GO.

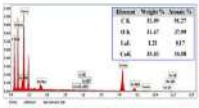

Figure 5: EDX pattern for identifying the ions' materials of the nanocomposites. EDX chemical analysis of cupric oxide (CuO), lanthanum oxide (La_2O_3), and graphene oxide GO composites (Table inset in Fig. 5)

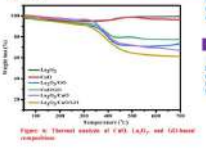

Figure 6: Thermal analysis of CuO, La_2O_3, and GO-based compositions

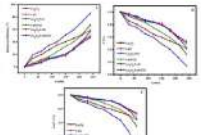

Figure 7: The degradation of methylene blue is studied at different times, and concentrations (A, B, and C).

Composition	Performance	Ref.
P-Chlorine/polyacrylonitrile/GO	80.10% Vs MB and 79.9% Vs MG dyes after irradiation time of 3 hr(s)	[110]
GO-manganese dioxide composites	Full Adsorption potential of MG and (1) MB (100%).	[111]
TiO_2-(x-2), GO composites	Dye disposal hits 98.25% in case of MB (30 min UV irradiation.)	[57]
CuO-ionic-liquid@GO fiber	82% of MB and 61% of hemoglobin	[112]
CuO and NiO_2	About 8 methylene blue dye 30.4%	[113]
Ferrihumate (ferric carbonate- doped clay) loving and reduced graphene oxide	Degradation of methyl orange efficiency 150 equal to 75.9%	[58]

Table 4: A number of recent results involve the mixed oxides NCs evaluation for water treatment purposes.

Conclusion

The effectiveness of the La_2O_3, CuO, and GO-based composite in removing methylene blue from wastewater has been demonstrated. A lanthana rod's length is typically 200 nm, according to TEM images. Additionally, FESEM micrographs show a decrease in the average grain size of CuO, which is 250 nm, and an enhanced porosity structure. Additionally, the roughness examination's results indicate a R_a value of 7.6 nm. TGA-DTA study further supports the potential for thermal stability. The binary NCs exhibit notable stability from ambient temperature to 700 oC; the residuals for La_2O_3/CuO, La_2O_3/CuO, and CuO/GO were 67%, 72%, and 77.5%, respectively. To verify the increased ecological application potential, the ternary nano-composite was tested for dye removal. The results show a maximum value of 89% for TNC as dye removal capability. As a result, the catalyst CuO/La_2O_3/GO NC might be recommended for the water treatment process.

References

Mohammed N. Almarri, Mai H. Khaled, M. Gouda, Hany M. Abd El-Lateef, Chemical, surface, and thermal studies of mixed oxides cupric oxide (CuO), lanthanum oxide (La_2O_3), and graphene oxide for dye degradation from aqueous solution, Journal of Materials Research and Technology, 21, 2022, 3265-3274.

On-Road Smart Charging System for Electric Vehicles

Hanoen AlHassan
Dr Mohammed AlAqil
Paper
Renewable Energy Track

Abstract

-Electric Vehicle charging could be done statically or dynamically. To improve EVs' and sustain the environment. Dynamic charging method like "wireless charging" are used. The main principle of wireless charging is to transmit power with the help of by electromagnetic field between the coils. By using this inductive power transfer battery are recharged through transformer winding placed at the bottom of car and other placed under the road. This would greatly increase the range of EV making it suitable for long drive & efficient too. This paper specially presents an evaluation on how future EV development and Wireless charging methods can be implemented on smart highway.

Introduction

In the current scenario global Warming and climate change Cars are a major reason for what's happening as gasoline-powered car exhaust directly affects global warming and the environment, so electric vehicle could play a vital role and new charging methods like "wireless charging" could help promote the same. With the help of Wireless charging, the EVs could be charged while driving, so frequently stopping at a station for charging is greatly reduced. This is due to the fact that one of the downsides of electric vehicles using wired charging needs a relatively long time during the charging process . The dynamic charging system would complete transition the electric vehicle industry making efficient and most importantly sustainable for environment.

Materials and Methods

The wireless EV charging on smart highway consists of 2 major components that are:

(A) INPUT POWER SUPPLY

Input to the system is obtained from 3 renewable source of energy that are Solar energy, wind energy, Noise energy. All the source are connected in series with rectifier circuit so as to get DC. As There output and to charge the battery bank and also restricts the reverse flow of power. All the source are connected in parallel.

(B) BATTERY BANK

[Li-ion Batteries connected in series having 4V each are connected in parallel

to each of our sources, which supplies power to automatic street light modules & wireless En charging module.

(C) WIRELESS EV CHARGING MODULE

It consists of a pair of high frequency transmitter and high frequency receiver coil. The high frequency transmitter coils are installed on the highway to provide wireless charging and the frequency receiver coil is installed in EV with a battery bank to store the energy transmitted wireless to run the vehicle in the absence of charging points.

Results

With increasing power level the percentage of road coverage to achieve the required driving range of 400 km decreases, however, the investment costs per km of installed on-road charging infrastructure increases.

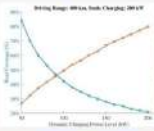

Safety and Insurance

In this project, the distances between the coils must be taken into account. All the signals are covered by an electromagnetic field because the presence of empty spaces from time to time may cause negativity on the battery.

Discussions

The economic viability of on-road wireless charging of electric vehicles (EVs) strongly depends on the choice of the inductive power transfer (IPT) system configuration (static or dynamic charging), charging power level and the percentage of road coverage of dynamic charging. In this paper, a case study is carried out to determine the expected investment costs involved in installing the on-road charging infrastructure for an electric bus fleet. Firstly, a generic methodology is described to determine the driving range of any EV (including electric buses) with any gross mass and frontal area.

A dynamic power consumption model is developed for the EV, taking into account the rolling friction, acceleration, deceleration, aerodynamic drag, regenerative braking and Li-ion battery behavior. Based on the simulation results, the linear dependence of the battery state of charge (SoC) on the distance traveled is shown. Further, the impact of different IPT system parameters on driving range is investigated. Economic evaluations of a combination of different IPT system parameters are explored for achieving the required driving range of 400 km, and the most optimized solution is presented for the case study of an electric bus fleet. It is shown that the choice of charging power level and road coverage are interrelated in the economic context. The economic viability of reducing the capacity of the on-board battery as a trade-off between higher transport efficiency and larger on-road charging infrastructure is presented.

Finally, important considerations, like the number of average running buses, scheduled stoppage time and on-board battery size, that make on-road charging an attractive option are explored. The cost break-up of various system components of the on-road charging scheme is estimated, and the final project cost and parameters are summarized. The specific cost of the wireless on-road charging system is found to be more expensive than the conventional trolley system at this point in time. With decreasing battery costs and a higher number of running buses, a more economically-viable system can be realized.

A model of the electric circuit that represents the theory and the way the electricity is transmitted while charging the vehicle wired.

When transmitting power wirelessly, a wireless carrier connects to an energy source, transporting the energy field through interference with future areas, where power is converted into a usable electric current .

In this model, 5 transmitters (coils) are placed along the road while being connected to a power source. When a vehicle crosses This road , which carries a receiver (coil), an electromagnetic field is formed between the transmitter and the receiver, resulting in battery charge .

Smart Car Charging Machine on the Developer Street

We simulated the smart street that charges cars using the coil only to driving code it aim to develop the smart more. Smart turbines are placed along the road. When the car moves, the turbines move because of the wind caused by the car's movement, and the turbine movements charge the sellers, which in turn generate power in the sells.

Conclusion

- This project has outlined a comprehensive overview of wireless charging technology for EVs. WPT technology offers the possibilities for better energy performance, lower environmental impacts, lower life cycle cost, and more convenience and operational safety benefits in the public area. Introducing on-smart charging of EV mainly through wireless roads, and defending the charging station nearby and for this generating electrical energy by sources like wind, wind and noise vibrations.
- The thickness and type of wire used to make the coils will affect the intensity of the electromagnetic field
- When charging is wired, this will help reduce the number of electric charging stations, directly affecting the reduction of charging costs. It will also create a lot of empty spaces, which in turn will help increase the spaces of cities.

References

[1] Kumar, K., GUPTA, S., & NEMA, S. (2021, February). A review of dynamic charging of electric vehicles. In 2021 7th International Conference on Electrical Energy Systems (ICEES) (pp. 180-184). IEEE.
[2] Mude, K. N., Sambaturu, R., Raju, C., & Rao, M. (2016). Design and implementation of wireless coupling for electric bicycle WPT charging. Journal of Electromagnetic Waves and Applications, 30(11), 75-85.
[3] Sergio, A., Agrawal, N., Veer, S., Oliver, J. A., Cobos, J. A., & Huerner, M. (2015). A wireless charging system applying phase-shift and amplitude control to maximize efficiency and extractable power. IEEE Transactions on Power Electronics, 30(11), 6338-6348.
[4] Ning, P., Miller, J. M., Onar, O. C., White, C. P., & Marinus, L. D. (2013, March). A wireless charging system development for EV/PHEV. Aerospace Annual IEEE Applied Power Electronics Conference and Exposition (APEC) (pp. 3049-3053). IEEE.
[5] Zhang, X., Yuan, Z., Yang, Q., Li, Y., Zhu, J., & Li, Y. (2018). Coil design and efficiency analysis for dynamic wireless charging system for electric vehicles. IEEE Transactions on Magnetics, 55(7), 1-5.

Cellulose Acetate-Based Films Embedded with Magnesium Ortho-Vanadate, Magnesium Oxide, and Graphene Oxide for Wound Healing

Student Name: Almoor Y.A. Al Bosager
Supervisors : Dr. Hany Abd M. El-Lateef, Dr. M. Gouda
Chemistry Department, College of Science, King Faisal University
Paper Materials (2023), IF= 3,748, Q1
Green chemistry and sustainable development track

Abstract

A multifunctional nano-films of cellulose acetate (CA)/ magnesium ortho-vanadate (MOV)/ magnesium oxide/ graphene oxide wound coverage was fabricated. The composition was confirmed by XRD, FTIR, and EDX techniques. SEM micrograph of $Mg_3(VO_4)_2$/MgO/GO/CA film depicted that, there as a porous surface with flattened rounded MgO grains with an average size of 0.31 µm was observed. Regarding wettability, the binary composition of $Mg_3(VO_4)_2$/CA accepted the lowest contact angle of 28.15±5.8do, while pure CA represents the highest one of 47.89±5.4 °. The cell viability % amongst the range of 4.9 µg/ml of $Mg_3(VO_4)_2$/MgO/GO/CA to 91.77±3.21%, while 2.4 µg/ml showed 101.54±2.13%. The higher concentration of 9000 µg/ml exhibited a viability of 19.23%. The thermogravimetric analysis showed three main stages of degradation. The initial temperature started from room temperature to 209 °C with a weight loss of 12%. On the other hand, the second stage started from the final temperature of the first stage and end at 378 ° C with a weight loss of 52%. Finally, the last stage was from 273 to 472 ° C with 19% weight loss. The obtained results such as high hydrophilic behavior, high cell viability, surface roughness, and porosity due to the addition of nanoparticles in the CA membrane played a significant role in enhancing the biocompatibility and biological activity of the CA membrane. The enhancements in the CA membrane promoted it to be utilized in drug delivery and wound healing applications.

Introduction

The aim of this work is to design membranes from CA to be utilized in wound healing and drug delivery applications. Several nanoparticles have been added to the AC to enhance its properties and also to give it several more properties. Mg is chosen to be added to the membrane because it has appropriate mechanical properties and because it enhances the catalytic activity of many enzymes. On the other hand, the presence of vanadate in the scaffold is due to its ability to enhance the interaction with cellular proteins and its antibacterial activity. Meanwhile, GO exhibits suitable properties for wound healing applications such as its antibacterial activity, drug-binding capacity, mechanical properties, electrical conductivity, and hydrophilic behavior. The unique properties of these nanoparticles make it a good choice to be embedded in the CA membrane for wound healing applications.

Materials and Methods

Preparation of Scaffold with Different Contents of Oxides Magnesium ortho-vanadate/ magnesium oxide and CA are taken from ZnO Ante. Additionally, GO is prepared in the laboratory by a modified Hummers' method [26,29]. Moreover, the CA films were formed with the casting methodology. To prepare the films, about 10 g of CA powder were dissolved in 100 mL of acetone under stirring as stock solution. The first sample was pure CA films, so about 20 mL of CA solution was poured into a Petri dish to dry the polymeric solution at a drier furnace. On the other hand, the second sample was prepared by injecting 20 mL of CA in a bottle under magnetic stirring then about 0.25 g of $Mg_3(VO_4)_2$ was wisely added to the solution. After an hour of stirring, the $Mg_3(VO_4)_2$ nanoparticles have been well dispersed in the solution. Then the second sample was poured into a Petri dish and dried. Furthermore, the third sample was obtained by adding 0.25 g of MgO nanoparticles to 20 mL of CA solution and stirring for 60 min. After that, the solution was poured into a Petri dish and dried. Moreover, the fourth sample was prepared by adding 0.125 g of $Mg_3(VO_4)_2$ to the polymeric solution under stirring, followed by approximately 0.125 g of MgO added to the same solution. After dispersing the nanoparticles in the CA solution, the solution was poured into a dish and dried. Finally, the last sample was prepared with three additives to 20 mL of CA. These additives 0.1 of $Mg_3(VO_4)_2$, 0.1 g of MgO, and 0.05 g of GO were separately added to the CA solution sequentially as dispersed using magnetic stirring. After that, the solution was poured and dried to obtain the film. The name of the cellulose acetate film was FAC.

Results and Discussions

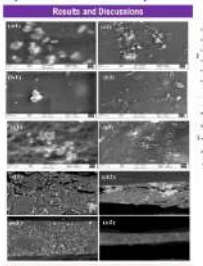

Figure 1: SEM of CA films with a variation of dopants where : (a), a)Mg3(VO4)2/CA film, (b), b)(Mg3 (VO4)2/MgO/CA, (c), c)(Mg3 (VO4)2/MgO/GO/CA, (d), d)) the cross-section of Mg3 (VO4)2/MgO/CA, (e), e)) the cross-section of Mg3 (VO4)2/MgO/GO/CA.

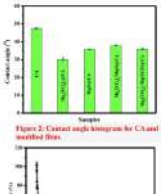

Figure 2: Contact angle histogram for CA and modified films

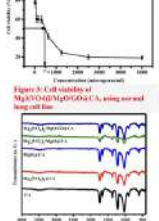

Figure 3: Cell viability of $Mg_3(VO_4)_2$/MgO/GO/CA/CA, using normal lung cell line

Figure 4: FTIR analysis of CA-based films

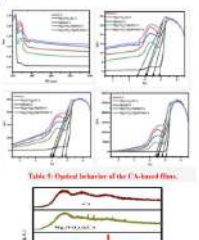

Table 5: Optical behavior of the CA-based films.

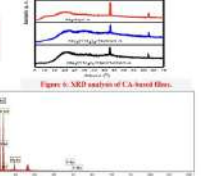

Figure 6: XRD analysis of CA-based films.

Figure 7: EDAX of $Mg_3(VO_4)_2$/MgO/GO/CA film

Conclusion

Multifunctional nano-films are fabricated by using cellulose acetate/ magnesium ortho-vanadate (MOV)/ magnesium oxide/ graphene oxide for wound healing applications. SEM micrograph of $Mg_3(VO_4)_2$/MgO/GO/CA film introduces the porous film with flattened rounded MgO grains with an average size of 0.31 µm. Concerning wettability, the binary composition of $Mg_3(VO_4)_2$/CA occupies the lowest contact angle at 28.15 ± 8.8do, while pure CA represents the uppermost one at 47.89 ± 5.4o. The cell viability ratio amongst the range of 4.9 µg/ml of $Mg_3(VO_4)_2$/MgO/GO/CA to 91.77 ± 3.2%, while a higher concentration of 9000 µg/ml exhibits viability of 19.23 ± 2.1%. Optically, the refractive index flees from 1.73 for pure polymer CA to 1.81 for $Mg_3(VO_4)_2$/MgO/GO/CA film. The thermal analysis showed three main degradation regions. The initial temperature of the first stage was 30 oC, and the final temperature was 209 oC. The peak temperature of this stage was 64.6oC with a 13% Wt. loss. On the other hand, the second stage existed in the range from 209 to 378 oC with a weight loss of 52%. Further, the last stage occurred from 378 to 472 oC with a Wt. loss of 19%. The residue was about 16% from the initial Wt. The obtained results exhibit improvements in structural, thermal, and optical integrity that offer superior biocompatibility.

References

Almoor, Y.A. Al Bosager, Hanie E. A. Algethami, M. Gouda, Hany M. Abd El-Lateef, Magnesium ortho-vanadate / magnesium oxide/ graphene oxide embedded through cellulose acetate-based films for wound healing application, Materials 2022, 15(6), 2099; https://doi.org/10.3390/ma15062099.

Out-patient clinic screening for anemia with non-invasive spectrophotometric hemoglobin concentrations compared to laboratory hemoglobin among sickle cell disease patients. A prospective observational study.

فحص مرضى العيادات الخارجية لفقر الدم مع تركيز الهيموجلوبين اللا اختراقي مقارنة بالهيموجلوبين المختبري بين مرضى فقر الدم المنجلي: دراسة ملاحظة مستقبلية

هوله سعيد بوعيلة مدارس نورة الجبر
رانيه أحمد الحلبي الكلية الطبية جامعة الملك فيصل
خالد أحمد بن
أستاذ التأثير كلية الطب جامعة الملك فيصل

Hereditary Blood Center, AlAhsa Research team:
Fatima Al Hamad, Nawal Eltayeb, Abdulazeiz Bushehab
KFU Statistics: Sayed Ali

Introduction

Patients with Sickle Cell Disease (SCD) frequently require venous blood sampling for hemoglobin (Hb) during out-patient clinic visits, which can be difficult and uncomfortable, particularly among young age groups. Primary aim is to monitor noninvasive spectrophotometric haemoglobin (SpHb, g/dl) concentration among SCD patients during their routine clinic visit and study their ability to screen for anemia compared to laboratory haemoglobin (Hb, g/dl). Secondary aim is to study the SpHb readings in relation to perfusion index (PI) and pleth variability index (PVI, %).

Materials and Methods

Approved by Al-Ahsa health Cluster (IRB KFHH No H-05-HS-065) IRB Log No: 06-HS-2023. Patients suffering from SCD visiting the Hereditary blood disease center in Al-Ahsa for follow up were included. SpHb, Pleth variability Index (PVI, %) and Perfusion Index (PI) measured via finger probe sensors (Masimo Radical 7, Irvine, CA, USA). Figure 1.
PI = AC/DC x 100% and by using PI, PVI is calculated: PVI =Pmax−Pmin/ Pmax X 100%. Figure 2.
Laboratory Hb measured by Abbott CELL-DYN Ruby hematology analyzer (Abbott, Abbott Park, Illinois, USA).Figure2. Study time: During routine follow-up visit to the clinics. P < 0.05 indicates statistical significance.

Figure 1: Masimo Radical 7 pulse oximeter.

Figure 2: Graphic representation of two wavelength signal processed internally by the pulse oximeters, where AC represents the variable absorption of infrared light due to pulsating arterial blood flow and DC represents the constant absorption of infrared light due to skin and other tissues.

Figure 3 : Abbott CELL-DYN Ruby hematology analyzer (Abbott, Abbott Park, Illinois, USA).

Figure 4

Results

- 170 patients were enrolled (369 Jun- 1st May 2023).
- Table 1, demonstrated low PI values among this group of SCD patients with a mean (SD) of 2.52+1.7, 2.5 and high mean PVI = 16.13 + 7.09 %.
- A weak correlation existed between PVI (%) and SpHb (g/dl), r = 0.049, p=0.54, while low correlation existed between PI and SpHb (r=0.36, p<0.001).
- SpHb overestimated hemoglobin with a mean difference or bias (SpHb-Hb) of 0.82 g/dl. (SD 1.29) and range (−3.1 to 4.2). The mean (SD) SpHb concentration (11.10 + 1.43 g/dl) was consistently higher than the mean (SD) of laboratory Hb (10.27 + 1.33 g/dl.), p<0.001. Figure 5.
- This mean difference (bias) (SpHb–Hb) increases with higher PI values as in Figure 6a.
- Mean (SpHb–Hb) inversely correlate with higher Hb. Figure 6b. Both illustrated by a nonparametric smoothed regression line. Figure 6a,b
- Table 2 and figure 7 a,b and c demonstrate the ability of SpHb to detect anemia. Hb below 13 g/dl, for males and 12 g/dl, for females, but at a low sensitivity of 64 for males and 78.6 for females.
- SpHb had the ability to detect anemia among 81.8 % of males with SCD and 91.3 % of females with SCD.

Table 1 and 2 Demographics and laboratory data. Mean of Hb ± was not different with Hydroxy Urea or not.

Figure 5: Dots plot with estimated log-lines for studies and 95% confidence interval (CI) of both (SpHb, g/dl and Hb, g/dl). With Mixture Signed Rank test performed.

Figure 6a: Relationship between bias (SpHb-Hb) and (PI). The trend illustrated by a nonparametric smoothed regression line.

Figure 6b: Relationship between bias (SpHb-Hb) and hb. Hb inversely correlated with high Hb.

Table 3: CBC Hb: hemoglobin concentration as measured by complete blood count, SpHb: non-invasive spectrophotometric measurement of Hb, hemoglobin concentration, CBC: complete blood count, NPV: Negative Predictive Value, PPV: Positive Predictive Value, AUC: Area Under Curve, WHO: World Health Organization criteria for anemia (Hb <11g/dl in females and Hb <13g/dl in males)

Figure 7 a: Receiver operating characteristic curves for (SpHb) detection of anemia among SCD males. SpHb cut-off value to detect anemia males is 11.7 g/dl.

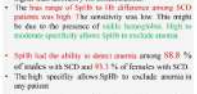

Figure 7 b: Receiver operating characteristic curves for (SpHb) detection of anemia among SCD females. SpHb cut-off value to detect anemia females is 11.2 g/dl.

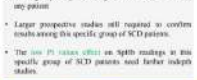

Figure 7 c: Receiver operating characteristic curves for (SpHb) detection of anemia among SCD males and females. No statistical significant difference, P 0.94.

Conclusion

- SpHb values over estimated lab Hb and was consistently higher than laboratory Hb concentrations.
- The bias range of SpHb to Hb difference among SCD patients was high. The consistency was low. This might be due to the presence of sickle hemoglobin. Hight to moderate specificity allows SpHb to exclude anemia.
- SpHb had the ability to detect anemia among 88.8 % of studies with SCD and 91.3 % of females with SCD.
- The high specificity allows SpHb to exclude anemia to any patient
- Larger prospective studies still required to confirm results among this specific group of SCD patients.
- The low PI values affect on SpHb readings in this specific group of SCD patients need further indepth studies.

References

1. Nahar SF, Hussain T, Tanang Derbile E, Ahmed Chowdhury M, Mahmud I. Hemoglobin levels in blood donors: sample study. 2018;10. 2(2):170-72 and 10.1515/jtim-2018-0025 PMID: 29922730 PMCID: PMC6004784
2. Strickland SM, Allen SL, Appiagyei BO, Bell-Peralta J. The accuracy of noninvasive and continuous total hemoglobin measurement by pulse CO-oximetry in screening for anemia. Anesth Analg. 2020 Dec; 131(6):1824-30. doi: 10.1213/ANE.0000000000004844. PMID: 32889867
3. Adam T, Pisarenko S, Cotes C, Kopec AS, Berkman LM. Evaluation of Noninvasive and Continuous Hemoglobin Monitoring in Children with Sickle Cell Disease. Proceedings of the 2015 Annual Meeting of the American Society of Anesthesiologists. 2015.
4. Mahmoud MK, Al-Salloom A, Alsaeed J, Al-Dabbagh AM, Alhamad AF, Al-Kenawy O, Qari S. Validation of a Non-Invasive Hemoglobin Measurement in Patients with Sickle Cell Disease. Blood 2015; 126 (23): 4778. doi: https://doi.org/10.1182/blood.V126.23.4778.4778
5. Nicholson T, Bell A, Jones-Knapp MJ, Tapuria N, Grant C, Zemaitis M, Bal U. Noninvasive Hemoglobin Measurement Has Poor Accuracy in Preoperative Patients Undergoing Elective Surgery. Anesthesiology Research and Practice. 2018 May 16;2018:1-10. 10.1155/2018/3027252 PMID: 29849615 PMCID: 5937600

ثانياً: الأوراق العلمية

م	المسار	عدد الاوراق	الاوراق المنشورة
1	الذكاء الاصطناعي في الطب (الجراحة)	1	
2	طب التخدير	2	
3	الهندسة والتصنيع والبناء	1	
4	الكيمياء	2	1
5	الفيزياء	2	
6	التقنية الحيوية	1	
7	الطاقة المتجددة	2	
	اجمالي الأوراق العلمية	11	1

ثالثاً: براءات الإختراع

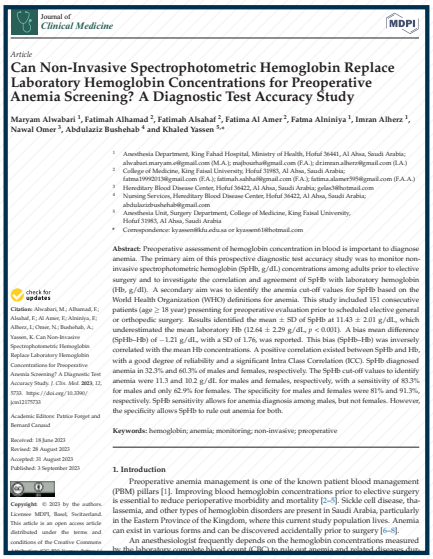

Journal of Clinical Medicine

MDPI

Article

Can Non-Invasive Spectrophotometric Hemoglobin Replace Laboratory Hemoglobin Concentrations for Preoperative Anemia Screening? A Diagnostic Test Accuracy Study

Maryam Alwabari [1], Fatimah Alhamad [2], Fatimah Alsahaf [2], Fatima Al Amer [2], Fatma Alniniya [3], Imran Alherz [3], Nawal Omer [3], Abdulaziz Bushehab [4] and Khaled Yassen [5,*]

materials

MDPI

Article

Magnesium Ortho-Vanadate/Magnesium Oxide/Graphene Oxide Embedded through Cellulose Acetate-Based Films for Wound Healing Applications

Fatemah A. Taher [1], Mohamed Gouda [1,*], Mai M. Khalaf [1,2], Saad Shaaban [1,3], Alnoor Y. A. Al Bosager [4], Dania A. A. Algafly [4], Metwally K. Mahfouz [5], Manal F. Abou Taleb [6] and Hany M. Abd El-Lateef [1,2,*]

microorganisms

MDPI

Article

The Halotolerant Probiotic Bacterium *Enterococcus lactis* ASF-2 from Al-Asfar Lake, Saudi Arabia, Reduces Inflammation in Carrageenan-Induced Paw Edema

Najla Alsaud [1], Amjad Almajed [2], Allujayn Lwusaybie [3], Aljawharah Alsubaie [3], Hela Alobaidan [3], Jihad Alessa [4], Abeer Almousa [4], Hairul Islam M. Ibrahim [4,5] and Ashraf Khalifa [4,6,*]

م	المسار	عدد براءات الإختراع	رقم التسجيل
1	الذكاء الاصطناعي في الطب (الجراحة)	**1**	
2	طب التخدير	**0**	
3	الهندسة والتصنيع والبناء	**0**	
4	الكيمياء	**2**	مجال معالجة الماء- رقم الطلب 18/139.461. مجال خلايا الوقود - رقم الطلب 33102.29
5	الفيزياء	**0**	
6	التقنية الحيوية	**1**	
7	الطاقة المتجددة	**0**	
	اجمالي البراءات	**4**	

رابعاً: المنتجات القابلة للتتجير

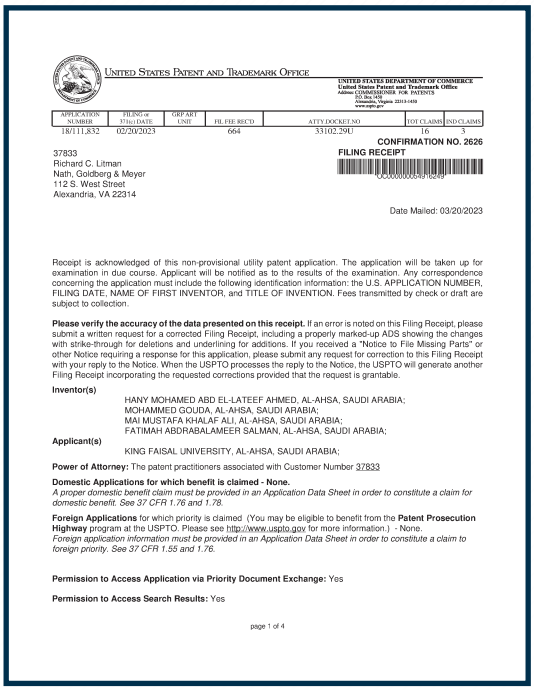

UNITED STATES PATENT AND TRADEMARK OFFICE

UNITED STATES DEPARTMENT OF COMMERCE
United States Patent and Trademark Office
Address: COMMISSIONER FOR PATENTS
P.O. Box 1450
Alexandria, Virginia 22313-1450
www.uspto.gov

APPLICATION NUMBER	FILING or 371(c) DATE	GRP ART UNIT	FIL FEE REC'D	ATTY.DOCKET.NO	TOT CLAIMS	IND CLAIMS
18/111,832	02/20/2023		664	33102.29U	16	3

CONFIRMATION NO. 2626

37833
Richard C. Litman
Nath, Goldberg & Meyer
112 S. West Street
Alexandria, VA 22314

FILING RECEIPT

Date Mailed: 03/20/2023

Receipt is acknowledged of this non-provisional utility patent application. The application will be taken up for examination in due course. Applicant will be notified as to the results of the examination. Any correspondence concerning the application must include the following identification information: the U.S. APPLICATION NUMBER, FILING DATE, NAME OF FIRST INVENTOR, and TITLE OF INVENTION. Fees transmitted by check or draft are subject to collection.

Please verify the accuracy of the data presented on this receipt. If an error is noted on this Filing Receipt, please submit a written request for a corrected Filing Receipt, including a properly marked-up ADS showing the changes with strike-through for deletions and underlining for additions. If you received a "Notice to File Missing Parts" or other Notice requiring a response for this application, please submit any request for correction to this Filing Receipt with your reply to the Notice. When the USPTO processes the reply to the Notice, the USPTO will generate another Filing Receipt incorporating the requested corrections provided that the request is grantable.

Inventor(s)

HANY MOHAMED ABD EL-LATEEF AHMED, AL-AHSA, SAUDI ARABIA;
MOHAMMED GOUDA, AL-AHSA, SAUDI ARABIA;
MAI MUSTAFA KHALAF ALI, AL-AHSA, SAUDI ARABIA;
FATIMAH ABDRABALAMEER SALMAN, AL-AHSA, SAUDI ARABIA;

Applicant(s)

KING FAISAL UNIVERSITY, AL-AHSA, SAUDI ARABIA;

Power of Attorney: The patent practitioners associated with Customer Number 37833

Domestic Applications for which benefit is claimed - None.
A proper domestic benefit claim must be provided in an Application Data Sheet in order to constitute a claim for domestic benefit. See 37 CFR 1.76 and 1.78.

Foreign Applications for which priority is claimed (You may be eligible to benefit from the **Patent Prosecution Highway** program at the USPTO. Please see http://www.uspto.gov for more information.) - None.
Foreign application information must be provided in an Application Data Sheet in order to constitute a claim to foreign priority. See 37 CFR 1.55 and 1.76.

Permission to Access Application via Priority Document Exchange: Yes

Permission to Access Search Results: Yes

page 1 of 4

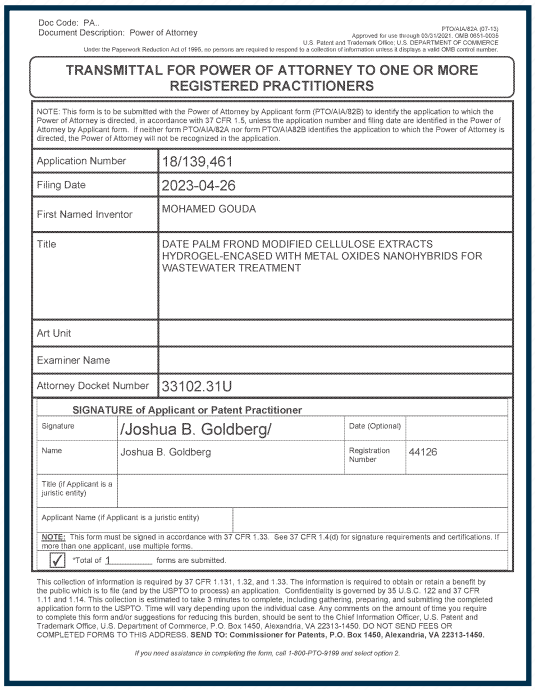

Doc Code: PA..
Document Description: Power of Attorney

PTO/AIA/82A (07-13)
Approved for use through 03/31/2021. OMB 0651-0035
U.S. Patent and Trademark Office; U.S. DEPARTMENT OF COMMERCE
Under the Paperwork Reduction Act of 1995, no persons are required to respond to a collection of information unless it displays a valid OMB control number.

TRANSMITTAL FOR POWER OF ATTORNEY TO ONE OR MORE REGISTERED PRACTITIONERS

NOTE: This form is to be submitted with the Power of Attorney by Applicant form (PTO/AIA/82B) to identify the application to which the Power of Attorney is directed, in accordance with 37 CFR 1.5, unless the application number and filing date are identified in the Power of Attorney by Applicant form. If neither form PTO/AIA/82A nor form PTO/AIA82B identifies the application to which the Power of Attorney is directed, the Power of Attorney will not be recognized in the application.

Application Number	18/139,461
Filing Date	2023-04-26
First Named Inventor	MOHAMED GOUDA
Title	DATE PALM FROND MODIFIED CELLULOSE EXTRACTS HYDROGEL-ENCASED WITH METAL OXIDES NANOHYBRIDS FOR WASTEWATER TREATMENT
Art Unit	
Examiner Name	
Attorney Docket Number	33102.31U

SIGNATURE of Applicant or Patent Practitioner

Signature	/Joshua B. Goldberg/	Date (Optional)	
Name	Joshua B. Goldberg	Registration Number	44126
Title (if Applicant is a juristic entity)			
Applicant Name (if Applicant is a juristic entity)			

NOTE: This form must be signed in accordance with 37 CFR 1.33. See 37 CFR 1.4(d) for signature requirements and certifications. If more than one applicant, use multiple forms.

☑ *Total of 1 forms are submitted.

This collection of information is required by 37 CFR 1.131, 1.32, and 1.33. The information is required to obtain or retain a benefit by the public which is to file (and by the USPTO to process) an application. Confidentiality is governed by 35 U.S.C. 122 and 37 CFR 1.11 and 1.14. This collection is estimated to take 3 minutes to complete, including gathering, preparing, and submitting the completed application form to the USPTO. Time will vary depending upon the individual case. Any comments on the amount of time you require to complete this form and/or suggestions for reducing this burden, should be sent to the Chief Information Officer, U.S. Patent and Trademark Office, U.S. Department of Commerce, P.O. Box 1450, Alexandria, VA 22313-1450. DO NOT SEND FEES OR COMPLETED FORMS TO THIS ADDRESS. **SEND TO: Commissioner for Patents, P.O. Box 1450, Alexandria, VA 22313-1450.**

If you need assistance in completing the form, call 1-800-PTO-9199 and select option 2.

م	المسار	عدد المنتجات
1	الذكاء الاصطناعي في الطب (الجراحة)	1
2	طب التخدير	1
3	الهندسة والتصنيع والبناء	2
4	الكيمياء	1
5	الفيزياء	0
6	التقنية الحيوية	1
7	الطاقة المتجددة	2
	اجمالي المنتجات	8

حجم التفاعل والظهور الإعلامي
حجم الظهور في منصة تويتر

87 منشورًا

حجم التفاعل والظهور الكلي
لحساب تويتر الجامعة

5,1 مليون

النشر الإعلامي لحسابات الجامعة الرسمية

تويتـــــر

الانستغرام

النشر الإعلامي لحساب البرنامج

تويتر

البنرات في موقع الجامعة الرسمي

أبرز تغريدات الصحف

المسار الرابع

أبرز تغريدات الجهات

أبرز تغريدات المغردين

علماء
المستقبل
يرحب بكم

علماء
المستقبل

جامعة الملك فيصل
KFU
KING FAISAL UNIVERSITY

مؤسسة عبدالمنعم الراشد الإنسانية
Abdulmonem Alrashed Humanitarian Foundation

علماء المستقبل

مؤسسة عبدالمنعم الراشد الإنسانية
Abdulmonem Alrashed Humanitarian Foundation

جامعة الملك فيصل
KFU
KING FAISAL UNIVERSITY

kfu.edu.sa